The Plant Cell, Vol. 17, 760–775, March 2005, www.plantcell.org © 2005 American Society of Plant Biologists

The Arabidopsis Plastidic Glucose 6-Phosphate/Phosphate Translocator GPT1 Is Essential for Pollen Maturation and Embryo Sac Development

Patrycja Niewiadomski,[a,1] Silke Knappe,[a,1] Stefan Geimer,[b] Karsten Fischer,[a] Burkhard Schulz,[c] Ulrike S. Unte,[d] Mario G. Rosso,[d] Peter Ache,[e] Ulf-Ingo Flügge,[a] and Anja Schneider[a,2]

[a] Botanisches Institut der Universität zu Köln, D-50931 Köln, Germany
[b] Biologie/Elektronenmikroskopie NW I/B1, Universität Bayreuth, D-95447 Bayreuth, Germany
[c] Zentrum für Molekularbiologie der Pflanzen, Universität Tübingen, D-72076 Tübingen, Germany
[d] Max-Planck-Institut für Züchtungsforschung, D-50928 Köln, Germany
[e] Julius-von-Sachs Institut für Biowissenschaften, Universität Würzburg, D-97082 Würzburg, Germany

Plastids of nongreen tissues can import carbon in the form of glucose 6-phosphate via the glucose 6-phosphate/phosphate translocator (GPT). The *Arabidopsis thaliana* genome contains two homologous *GPT* genes, At*GPT1* and At*GPT2*. Both proteins show glucose 6-phosphate translocator activity after reconstitution in liposomes, and each of them can rescue the low-starch leaf phenotype of the *pgi1* mutant (which lacks plastid phosphoglucoisomerase), indicating that the two proteins are also functional in planta. At*GPT1* transcripts are ubiquitously expressed during plant development, with highest expression in stamens, whereas At*GPT2* expression is restricted to a few tissues, including senescing leaves. Disruption of *GPT2* has no obvious effect on growth and development under greenhouse conditions, whereas the mutations *gpt1-1* and *gpt1-2* are lethal. In both *gpt1* lines, distorted segregation ratios, reduced efficiency of transmission in males and females, and inability to complete pollen and ovule development were observed, indicating profound defects in gametogenesis. Embryo sac development is arrested in the *gpt1* mutants at a stage before the fusion of the polar nuclei. Mutant pollen development is associated with reduced formation of lipid bodies and small vesicles and the disappearance of dispersed vacuoles, which results in disintegration of the pollen structure. Taken together, our results indicate that GPT1-mediated import of glucose 6-phosphate into nongreen plastids is crucial for gametophyte development. We suggest that loss of GPT1 function results in disruption of the oxidative pentose phosphate cycle, which in turn affects fatty acid biosynthesis.

INTRODUCTION

Nongreen plastids in heterotrophic tissues are carbohydrate-importing organelles, and in storage tissues amyloplasts are the site of starch synthesis. Nongreen plastids are normally unable to generate hexose phosphates from C3 compounds because they lack fructose 1,6-bisphosphatase activity (Entwistle and ap Rees, 1988), and they depend on the import of hexose phosphates as the source of carbon for starch biosynthesis and for the oxidative pentose phosphate pathway (OPPP). In all dicotyledonous species studied so far, nongreen plastids preferentially take up glucose 6-phosphate (Glc6P) as the hexose phosphate (Caspar et al., 1985; Kofler et al., 2000; for review, see Fischer and Weber, 2002). By contrast, in the endosperm of monocot cereals, starch biosynthesis preferentially employs ADP-glucose generated in the cytosol (Beckles et al., 2001), but these tissues also possess a Glc6P uptake system.

Indeed, the Glc6P/phosphate translocator (GPT) was first purified from plastid envelope membranes isolated from maize (*Zea mays*) endosperm (Kammerer et al., 1998), and corresponding cDNAs have since been isolated from various plant species (Kammerer et al., 1998). At the protein level, these GPTs display low, but significant, similarity to other subfamilies of plastidic phosphate antiport systems, namely, the triose phosphate/phosphate translocator (Flügge, 1999), the phospho*enol*pyruvate/phosphate translocator (Fischer et al., 1997), and the xylulose 5-phosphate/phosphate translocator (Eicks et al., 2002). The proposed physiological function of the GPT is the Glc6P import into plastids of heterotrophic tissues for use as a precursor for starch (and fatty acid) biosynthesis and/or as a substrate for the OPPP. The OPPP provides reducing equivalents for biosynthetic pathways that rely on reducing power, such as the synthesis of fatty acids (Bowsher et al., 1992). These reducing equivalents are used for the reduction of 3-ketoacyl-ACP to acyl-ACP, a reaction catalyzed by two subunits of the fatty acid synthase complex, 3-ketoacyl reductase and enoyl-ACP reductase. The activity of fatty acid synthase ultimately leads to the synthesis of saturated 16:0 and 18:0 fatty acids that are used for the synthesis of various glycerolipids, such as

[1] These authors contributed equally to this work.
[2] To whom correspondence should be addressed. E-mail anja.schneider@uni-koeln.de; fax 49-221-4705039.
The author responsible for distribution of materials integral to the findings presented in this article in accordance with policy described in the Instructions for Authors (www.plantcell.org) is: Anja Schneider (anja.schneider@uni-koeln.de).
Article, publication date, and citation information can be found at www.plantcell.org/cgi/doi/10.1105/tpc.104.029124.

phospholipids and triacylglycerol (for review, see Ohlrogge and Browse, 1995). Mutations that disrupt early steps in fatty acid biosynthesis are presumed to be lethal. Indeed, complete loss of function of the enzymes in this pathway is incompatible with viability (Mou et al., 2000; Carlsson et al., 2002; Baud et al., 2003).

In oilseed plants like *Arabidopsis thaliana*, a transient accumulation of starch during embryogenesis is followed by massive deposition of triacylglycerols, which are stored in oil bodies that account for ~60% of the cell volume in the cotyledons of mature embryos (Mansfield and Briarty, 1992). Changes in gene expression during seed development in Arabidopsis have been monitored by cDNA microarray analysis, and, interestingly, the expression of *GPT1* mRNA was found to correlate with the transient accumulation of starch and to decline rapidly 8 d after flowering (Ruuska et al., 2002).

Just as storage oil bodies accumulate in cotyledons, pollen grains also accumulate intracellular lipid bodies, which act as reserves of energy and biomolecules for pollen germination. The pollen grain—the male or microgametophyte—develops within the anther in the stamen. The postmeiotic haploid microspore undergoes an asymmetric mitosis (pollen mitosis I), which results in a vegetative and a generative cell. The generative cell then undergoes a second mitosis to form two sperm cells (for review, see Mascarenhas, 1989; Twell et al., 1998; McCormick, 2004). Likewise, the female gametophyte, also referred to as the megagametophyte or embryo sac, develops within the ovule, which is found within the ovary in the carpel. Female gametophyte development comprises three successive rounds of nuclear division, followed by cellularization. The result is a seven-cell embryo sac that contains three antipodal, two synergid, one egg, and one central cell (reviewed in Reiser and Fischer, 1993; Drews et al., 1998; Yadegari and Drews, 2004). Mitochondrial and plastid DNAs are inherited maternally in Arabidopsis (Röbbelen, 1966; Martinez-Zapater et al., 1992; Martinez et al., 1997); the organellar DNAs in the male generative cell are degraded in a process that starts just after the first pollen mitosis (Nagata et al., 1999). In the pollen grain, therefore, intact plastids are found only in the vegetative cell. Because the components of the fatty acid biosynthetic machinery are located within plastids, intracellular lipid biosynthesis in pollen grains can only take place in the vegetative cell under the control of the gametophytic genome. Intracellular lipid biosynthesis gives rise to storage lipid bodies and an extensive membrane network (for review, see Piffanelli et al., 1998). Both the membrane and storage lipids of pollen grains provide the substrates for the rapid expansion of the plasmalemma after pollen germination and the subsequent elongation of the pollen tube.

The Arabidopsis genome contains two *GPT* genes, At*GPT1* (*At5g54800*) and At*GPT2* (*At1g61800*) that resulted from a duplication and a subsequent translocation event that were independent of the segmental duplications identified in Arabidopsis and its progenitors (Knappe et al., 2003a). In this study, we report on the functional characterization of the two At*GPT* genes. Both GPTs are functional Glc6P translocators, but expression studies and the analysis of loss-of-function lines revealed that only GPT1 is essential. Mutations in *gpt1* result in severe defects, especially during pollen development, whereas loss of *GPT2* function has no obvious effect on plant development.

RESULTS

AtGPT1 and AtGPT2 Represent Functional Glc6P Translocators

To elucidate the functional characteristics of AtGPT1 and AtGPT2, cDNAs coding for the mature forms of both transporters were extended by a sequence coding for an N-terminal His_6 affinity tag, cloned into the yeast expression vector pYES2 NT, and transformed into yeast cells. Affinity-purified AtGPT1 and AtGPT2 were then reconstituted into liposomes, which had been preloaded with different metabolites for the subsequent determination of transport specificities (Loddenkötter et al., 1993). The substrate specificities of the two transporters are listed in Table 1. Both Arabidopsis GPTs proved to be functional Glc6P transporters with almost identical substrate specificities, transporting inorganic phosphate, Glc6P, 3-phosphoglycerate, triose phosphates, and, to a lesser extent, phospho*enol*pyruvate. In general, the transport specificities of the two Arabidopsis GPTs were similar to those of the GPT from pea (*Pisum sativum*) roots (PsGPT; Kammerer et al., 1998).

The plastidic phosphoglucose isomerase (PGI; EC 5.3.1.9) mutant *pgi1* provided an opportunity to study AtGPT1 and AtGPT2 transport function in planta. The *pgi1* mutant was isolated in a screen for leaf-specific starch deficiency (Yu et al., 2000). It retains only ~5% of wild-type plastid PGI activity (Yu et al., 2000), and its leaves contain ~25% of the wild-type level of starch (Figure 1). The plastid PGI converts Fru6P to Glc6P, which is then used as precursor for starch biosynthesis. Thus, if both GPTs represent functional Glc6P translocators, their ectopic expression in leaves should physiologically rescue the *pgi1*-specific starch deficiency phenotype by making cytosolic Glc6P available to chloroplasts as a precursor for starch biosynthesis. For this purpose, Ps*GPT*, At*GPT1*, and At*GPT2* cDNAs were stably expressed under the control of the 35S promoter in the *pgi1-1* mutant background. For each construct, four to five independent lines were selected and analyzed for their leaf starch phenotype (Figure 1). The *pgi1-1 35S:PsGPT* lines showed a dramatic increase in leaf starch (130% of wild-type levels), indicating that PsGPT indeed delivers Glc6P to plastids for starch biosynthesis. The *pgi1-1 35S:AtGPT1* and *pgi1-1 35S:AtGPT2* lines displayed 80 and 135% of wild-type starch levels, respectively (Figure 1). Furthermore, the slight growth

Table 1. Substrate Specificities of Recombinant GPTs Expressed in Yeast Cells

Transporter	Phosphate	Glc6P	3-PGA	PEP	TP
PsGPT	100	90 ± 9[a]	50 ± 1[a]	20 ± 1[a]	112 ± 5[a]
AtGPT1	100	116 ± 20	88 ± 9	35 ± 10	48 ± 14
AtGPT2	100	103 ± 5	61 ± 10	41 ± 4	106 ± 17

The liposomes were preloaded with 30 mM substrate as indicated. Transport of [^{32}P] phosphate is given as a percentage of the activity measured for liposomes preloaded with inorganic phosphate. Values are means of three to four experiments (±SE). 3-PGA, 3-phosphoglycerate; PEP, phospho*enol*pyruvate; TP, triose phosphate.
[a] Data from Kammerer et al. (1998).

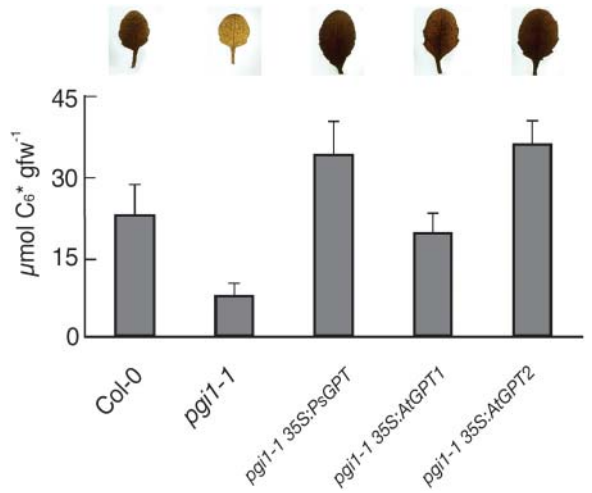

Figure 1. Rescue of the Defect in Starch Accumulation in the *pgi1-1* Mutant by Ectopic Expression of GPT.

The starch content of leaves of 4-week-old plants grown on a light/dark cycle of 12 h/12 h was determined at the end of the light period. Top panel, leaves stained with iodine; bottom panel, enzymatically determined starch content. The values are means for four to five different plants (±SD). fw, fresh weight.

retardation characteristic of the *pgi1-1* mutant was attenuated in each of the lines (data not shown). These experiments clearly demonstrate that both Arabidopsis proteins can deliver cytosolic Glc6P to the chloroplasts for starch biosynthesis, thus obviating the need for PGI. Therefore, both Arabidopsis GPTs represent functional GPTs in planta.

Tissue-Specific Expression Patterns of AtGPTs

To investigate the expression of At*GPT1* and At*GPT2*, publicly available microarray data were analyzed (https://www.genevestigator.ethz.ch/) (Zimmermann et al., 2004). At*GPT1* is ubiquitously expressed during development (e.g., in seeds, flowers, rosettes, and roots, with highest levels found in stamens) (Figure 2). In general, At*GPT2* is expressed at lower levels than At*GPT1*; however, relatively higher levels were detected in sepals and senescing leaves (Figure 2). Similar expression patterns were observed using RT-PCR (data not shown).

To gain a deeper insight into the tissue-specific expression of At*GPT1*, a translational fusion of the promoter sequence, the first exon and intron with the *uidA* gene, was stably introduced into Arabidopsis. *AtGPT1*:*uidA* expression was observed in leaf mesophyll and guard cells; β-glucuronidase (GUS) localization in mesophyll and guard cell chloroplasts was readily detectable (Figures 3A and 3B). To quantify *GPT1* expression in these two leaf tissues, protoplasts of mesophyll and guard cells were prepared and subjected to RT-PCR. As shown in Figure 3C, a 10-fold increase in the accumulation of *GPT1* transcripts was observed in guard cells relative to mesophyll cells. In roots, *AtGPT1*:*uidA* expression was restricted to the root cap, the vascular tissue, and the zone of lateral root formation (Figures 3D and 3E). In flowers, *AtGPT1*:*uidA* was expressed in pollen, as well as in the carpel, stigma, and the vascular tissue of sepals (Figure 3F). During early embryo development, *AtGPT1*:*uidA* expression was found throughout the whole seed, including the globular-stage embryo, the endosperm, and the integuments (Figures 3G and 3H). This ubiquitous expression pattern was also detected in early heart stage embryos (Figure 3I); however, during the late heart stage, *AtGPT1*:*uidA* expression began to disappear in the ground tissue (Figure 3J). At the transition to the torpedo stage, and in the mature embryo, *AtGPT1*:*uidA* expression was restricted to the root tip (Figures 3K and 3L). No expression was detected in mature seeds; only the pericarp showed weak *AtGPT1*:*uidA* expression (Figure 3M).

Isolation of Insertional Mutant Lines for *AtGPT1*

To identify *A. thaliana* lines that carry T-DNA insertions at the At*GPT1* locus, the Feldmann lines (Forsthoefel et al., 1992), the Arabidopsis Knockout Facility (AKF) BASTA population (Sussman et al., 2000), and the Salk Institute collection (Alonso et al., 2003) were screened by reverse genetics. In the Feldmann collection, two lines were identified, which harbored T-DNA insertions 586 bp upstream (*gpt1-5*) and 256 bp downstream (*gpt1-1*) of the start codon of At*GPT1*, respectively (Figure 4A). In the BASTA population from the AKF, two lines were identified that contained T-DNA insertions at positions +1725 (*gpt1-2*) and +2754 (*gpt1-6*), relative to the ATG (Figure 4A). In addition, two lines (*gpt1-3* and *gpt1-4*) were identified in the Salk collection, with T-DNA insertions at positions −19 and +1899 relative to the start codon of At*GPT1* (Figure 4A). To isolate homozygous mutant lines, different gene-specific primers were combined with the respective border primers for genotyping (Figure 4B). In the

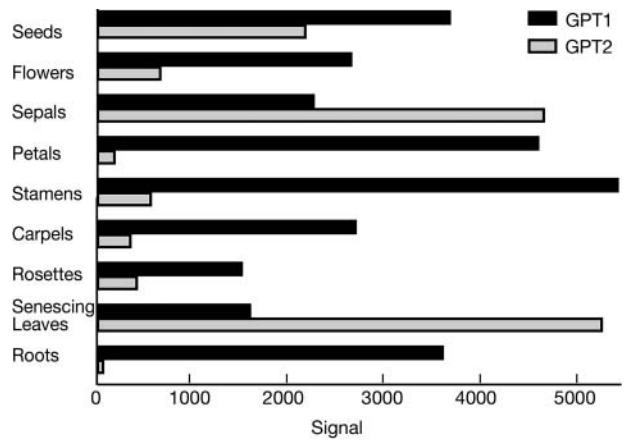

Figure 2. Digital Northern Analysis of At*GPT* Genes.

Data used to create the Digital Northern were obtained from AtGenExpress at the Genevestigator site (https://www.genevestigator.ethz.ch/). Signal intensities for seeds were averaged for stages 6 to 10, for flowers from stages 9 to 12 and 15, for sepals, petals, stamens, and carpels from stages 12 and 15, and for rosettes from rosette leaves 2 to 12. Mean signal intensities for senescing leaves and roots were averaged from the technical replicates only.

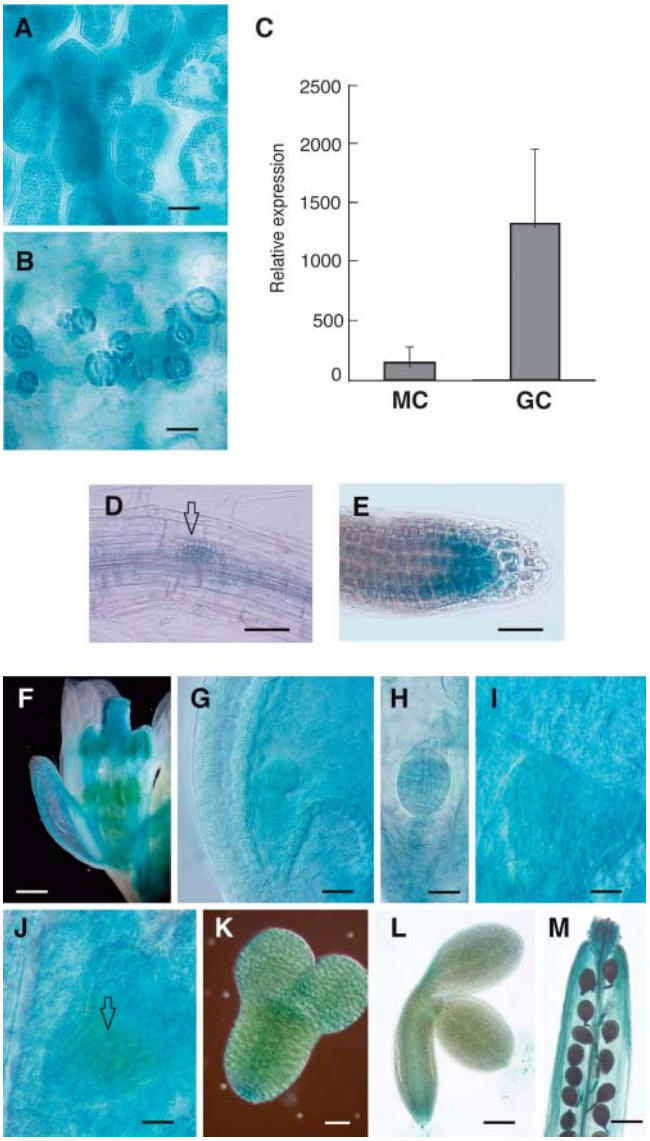

Figure 3. *GPT1*:*uidA* Expression in Transgenic Arabidopsis Plants.

(A) Rosette leaf of a 3-week-old plant with the plane of focus on mesophyll cells. Note the targeting of GUS protein to chloroplasts.
(B) Rosette leaf as in **(A)** with the plane of focus on guard cells.
(C) Quantitative RT-PCR analysis of mRNA from isolated mesophyll cells and guard cells. The amplification of *GPT1* cDNA was performed using primers GPT1-RT-F and GPT1-RT-R. The *AtGPT1* expression was normalized to 10,000 molecules of *Actin2*. The values shown are the means of three different experiments (±SD). MC, mesophyll cell; GC, guard cell.
(D) and **(E)** Primary root and root tip of an adult plant. Note GUS activity at the initiation site of the lateral root (indicated by an arrow in **[D]**) and in the root cap **(E)**.
(F) Cleared whole-mount preparation of a flower.
(G) to **(M)** Cleared whole-mount preparations of developing seeds harboring embryos at different developmental stages.
(G) Early globular stage embryo.
(H) Globular stage embryo.
(I) Early heart stage embryo.
(J) Heart stage embryo. The ground tissue is indicated by an arrow.
(K) Embryo at the transition from heart stage to torpedo stage.
(L) Mature embryo.
(M) Dissected silique containing mature seeds.
Bars = 25 μm in **(A)**, **(B)**, and **(G)** to **(K)**, 50 μm in **(D)** and **(E)**, 100 μm in **(L)**, and 500 μm in **(F)** and **(M)**.

lines *gpt1-3*, *gpt1-5*, and *gpt1-6*, homozygous mutant plants were clearly identified (Figure 4B). However, RT-PCR analysis revealed that *GPT1* expression was not impaired in these genotypes (data not shown). By contrast, no homozygous mutant lines could be obtained for *gpt1-1*, *gpt1-2*, or *gpt1-4* (Figure 4B).

Lines heterozygous for the *gpt1-1* or the *gpt1-2* mutation were chosen for further analysis. The heterozygous state of the lines was confirmed by DNA gel blot analysis using a gene-specific probe (Figure 4C). The filters were also hybridized with border-specific fragments. In the *GPT1*/*gpt1-1* line, the right border–specific probe detected a 9-kb fragment only, indicating the presence of a single-copy T-DNA insertion. In *GPT1*/*gpt1-2*, the left border–specific probe detected a 1.8-kb fragment, but additional bands were also present, indicating the presence of several T-DNAs or a complex of insertions. This line was back-crossed to the wild type. In the subsequent F2 generation, it was not possible to isolate a single-copy line that showed BASTA resistance, so a PCR-based assay was used to monitor the segregation of the *gpt1-2* allele in subsequent generations (see Methods).

Genetic Analysis and Complementation of *gpt1*

The progeny of line *GPT1*/*gpt1-1*, which contains a single-copy T-DNA insertion that confers kanamycin resistance (Kan^r), segregated 0.9:1 for Kan^r (Table 2). DNA gel blot analysis revealed that all Kan^r plants contained the T-DNA insertion in *GPT1* and were heterozygous at the *GPT1* locus (data not shown). A total of 393 offspring of selfed *GPT1*/*gpt1-2* plants was subjected to PCR analysis, and 176 lines were found to carry the *gpt1-2* allele (Table 2), indicating a 0.8:1 segregation, very similar to the aberrant segregation observed for the *gpt1-1* allele. The segregation ratios of both *gpt1-1* and *-2* were not significantly different from 1:1 (Table 2), instead of an expected 3:1, given the dominant mode of inheritance of both PCR and resistance phenotypes. The simplest explanation for the aberrant segregation patterns would be a gametophytic defect. To test this, male and female transmission efficiencies (TE) of the two defective *gpt1* alleles were determined by performing reciprocal test crosses between heterozygous mutants and wild-type plants and analyzing the F1 progeny. Both *gpt1-1* and *gpt1-2* alleles showed reduced male and female TEs (Table 3); for *gpt1-1*, a female TE of 34% and a male TE of 20% was determined. Similar values were observed for the *gpt1-2* allele: a female TE of 27% and a male TE of 20% in the test cross to Wassilewskija (Ws-2), and a female TE of 36% and a male TE of 24% in the test cross to Columbia (Col-0). Thus, the observed segregation ratio was not caused by a defect that is specific to the male or female line, but appeared to result from reduced TE through both gametophytes.

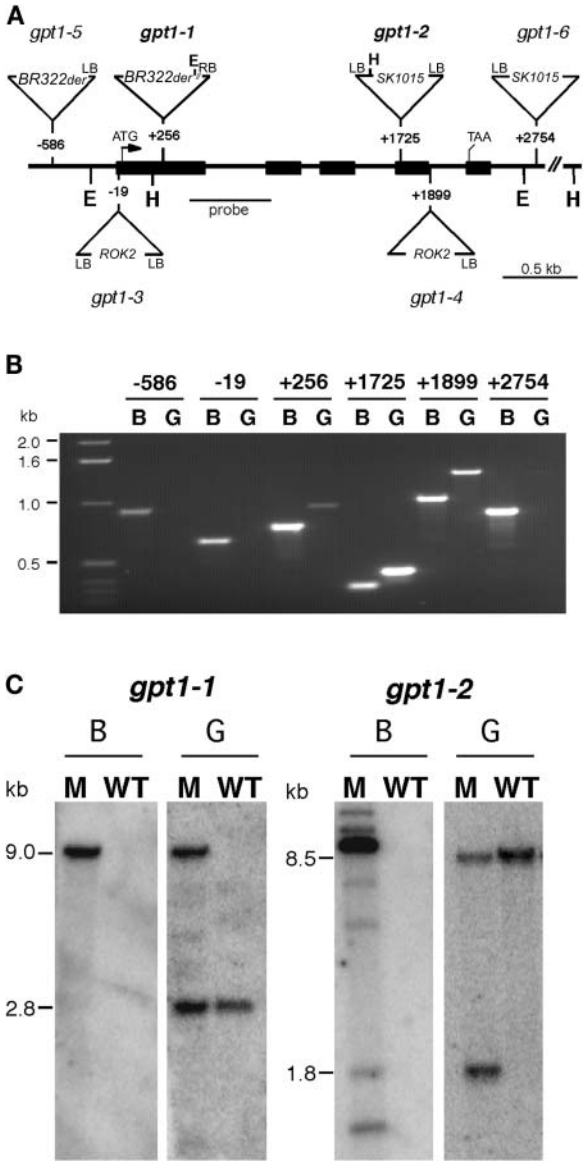

Figure 4. Identification and Molecular Characterization of *gpt1* Alleles.

(A) Exon/intron structure of the At*GPT1* gene showing the locations (relative to the start codon) of insertion sites identified in T-DNA mutants. The two alleles *gpt1-1* and *gpt1-2* used for further characterization are indicated in bold. LB, left border of the T-DNAs for which the precise integration sites could be identified; BR322der, T-DNA present in the Feldman collection; SKI015, T-DNA present in the AKF BASTA population; ROK2, T-DNA present in the Salk collection; E, *Eco*RI; H, *Hin*dIII; RB, right border.

(B) Genotyping of the six *gpt1* alleles by PCR. Information regarding primer combinations is provided in Methods. The absence of a gene-specific PCR amplification product indicates that the line is homozygous for the relevant mutation. The lines are designated by the position of the insertion site relative to the start codon. B, border- and gene-specific primer combination; G, gene-specific primer combination.

(C) DNA gel blot analysis of *GPT1/gpt1-1* and *GPT1/gpt1-2*. *Eco*RI-digested DNA (10 μg) of *GPT1/gpt1-1* and *Hin*dIII-digested DNA (10 μg) of *GPT1/gpt1-2*, together with the appropriate wild-type control DNA, were each successively hybridized with a border-specific and a gene-specific fragment. The gene-specific probe used for hybridization is indicated in **(A)**. The sizes of the wild-type fragments and the novel fragments in the heterozygous mutant lines are indicated. M, heterozygous mutant line; B, border-specific fragment; G, gene-specific fragment.

Analysis of siliques of *GPT1/gpt1-1* and *GPT1/gpt1-2* plants revealed the presence of small, white, unfertilized ovules (Figure 5A) with a frequency of 32 and 28%, respectively, whereas such aborted ovules occurred with a frequency of only 7% in the wild type (Table 4). Although the less densely packed siliques of the heterozygous lines were shorter than those of the wild type (1.12 ± 0.12 cm versus 1.52 ± 0.08), the overall seed set (normal seeds plus aborted ovule) per silique did not differ markedly between heterozygous *GPT1/gpt1-2* lines and wild-type plants (49 ± 5 versus 50 ± 7).

To complement the mutant phenotype, an 11-kb genomic fragment containing the *GPT1* gene, including promoter and terminator regions, was introduced into *GPT1/gpt1-2* plants. Nine independent T1 lines that inherited the *gpt1-2* allele were generated. All of these lines were still heterozygous at the endogenous *GPT1* locus (data not shown). Two lines (*gpt1-2/GPT1 gGPT1-3* and *gpt1-2/GPT1 gGPT1-9*) were further analyzed in the T2 generation for segregation of the *GPT1* locus using PCR. In each of the two T2 progenies, individual plants (8 out of 77 and 10 out of 28, respectively) were identified that were homozygous for the *gpt1-2* allele. DNA from two representative plants, *gpt1-2/gpt1-2 gGPT1-9.18* and *gpt1-2/gpt1-2 gGPT1-3.10*, was subjected to DNA gel blot analysis, and the homozygous state of the endogenous *gpt1* locus was confirmed (Figure 5B). Siliques of *gpt1-2/gpt1-2 gGPT1-9.18* and *gpt1-2/gpt1-2 gGPT1-3.10* plants were inspected for aborted ovules in the T3 generation. In both lines, the frequency of aborted ovules was comparable to that in wild-type plants (Table 4, Figure 5C). This result confirms that the T-DNA insertions in the *GPT1* gene were responsible for the lethal phenotype in the homozygous state and also increased the number of aborted ovules in siliques of heterozygous mutant plants.

Loss of GPT1 Function Perturbs Pollen Development

The reduction in TE via the male germ line in *gpt1* plants suggests a role for *GPT1* in pollen development and/or function. Pollen of wild-type and *GPT1/gpt1* lines was analyzed for cytoplasmic density by the staining method of Alexander and for nuclear constitution by 4′,6-diamidino-2-phenylindole (DAPI) staining. In the Alexander assay, vital mature pollen grains show intensive red staining of the cytoplasm (Figure 6A). Dead and dying pollen, recognizable by its flattened shape and smaller size, exhibited only green staining of the pollen grain wall (Figure 6B). In wild-type plants, inviable pollen grains occurred with a frequency of <1%, whereas in *GPT1/gpt1-1* and *GPT1/gpt1-2* plants, the frequency was between 9 and 15% (Table 4). In both complemented lines, *gpt1-2/gpt1-2 gGPT1-9.18* and *gpt1-2/gpt1-2 gGPT1-3.10*, the frequency of dead pollen was comparable to that in the wild type, confirming the importance of *GPT1* for pollen development

Table 2. Segregation Analysis of *GPT1/gpt1-1* and *GPT1/gpt1-2*

Genotype	Kan^r/PCR$^+$	Kan^s/PCR$^-$	Ratio	χ^2 (P)
GPT1/gpt1-1	190	222	0.9:1	2.5 (P = 0.01)
GPT1/gpt1-2	176	217	0.8:1	4.2 (P = 0.01)

The inheritance of *gpt1-1* was analyzed by counting kanamycin-resistant seedlings recovered from selfed *GPT1/gpt1-1* plants. The inheritance of *gpt1-2* was monitored using a PCR-based assay as described in Methods. The χ^2 test was used to compare the observed ratios with a predicted ratio of 1:1. Kan^r, kanamycin resistant; Kan^s, kanamycin sensitive.

(Table 4). The small and flattened pollen grains were further investigated for their nuclear constitution by staining with DAPI. In wild-type pollen, the vegetative nucleus and the two generative nuclei were clearly distinguishable (Figure 6C). In the mutant pollen, only diffuse staining was observed (Figure 6D). Besides this strong mutant phenotype, we observed several intermediate phenotypes in DAPI- and Alexander-stained pollen, which might result in inviability after release (data not shown).

Using scanning electron microscopy, pollen from wild-type and heterozygous *gpt1* lines was examined more closely. Pollen grains from the wild type appeared normal (Figure 6E), whereas significant numbers of abnormal and collapsed pollen grains were detected in the *GPT1/gpt1* lines (Figure 6F), which is consistent with our light microscopic observations (Figures 6A to 6D). Although the mutant pollen grains were smaller in size and less robust, the ordered reticulate pattern of the wild-type exine layer was still prominent (Figures 6G and 6H), indicating that the basic structure of the exine layer is not altered. The exine layer is produced by the sporophytic tissue, which suggests that the heterozygous tissue of the sporophyte has no influence on the development of *gpt1* mutant pollen.

Pollen Grains Harboring the *gpt1* Allele Have Fewer Vacuoles and Lipid Bodies and Show a Tendency to Lyse

To define the time point of *gpt1* pollen grain collapse, the expression of *GPT1*:*uidA* was investigated. *GPT1*:*uidA* expression was readily detected in tricellular pollen grains (Figures 7A and 7B), whereas GUS activity could not be unequivocally demonstrated in uninuclear und bicellular pollen (data not shown). This *GPT1*:*uidA* expression profile is in good agreement with publicly available microarray data (Figure 7C), which show that *GPT1* expression levels are highest in tricellular pollen.

Cross sections of wild-type and *GPT1/gpt1-2* anthers, analyzed by transmission electron microscopy, revealed that development of the pollen sac, including its tapetum layer, was similar in the two genotypes (data not shown). The *gpt1-2* defect was evident in pollen sacs of *GPT1/gpt1-2* anthers (anther stage 12, according to Sanders et al., 1999) harboring mature tricellular pollen grains (Figure 8A). At this stage, the tapetal cell layer has almost completely disappeared, and degeneration of the septum gives rise to a bilocular anther. Within the locule of the pollen sac, a mixture of pollen grains was found. Wild-type–like pollen grains within the *GPT/gpt1-2* locule were identified by the presence of lipid bodies and vacuoles (Figure 8B). The mutant pollen grains showed varying degrees of damage and could be grouped into three classes (weak, moderate, and strong). Weakly affected mutant pollen still has intracellular structures but lacks vacuoles (Figure 8C). In addition, significantly fewer lipid bodies were present in cross sections of mutant pollen (25 $\pm$ 5.8) compared with 72 $\pm$ 15.4 lipid bodies in cross sections of wild-type pollen (*t* test, P < 0.001). In agreement with the observations made by light microscopy, a significant proportion of mutant pollen grains were collapsed (Figure 8D). The endothecial cells of the heterozygous *GPT1/gpt1-2* tissue contained plastids with starch granules and plastoglobuli and therefore exhibited a wild-type–like phenotype (Figure 8D). Similar observations were made with the *GPT1/gpt1-1* line (data not shown).

Besides the prominent constituents of wild-type pollen grains, namely, the lipid bodies and the vacuoles (possibly storage vacuoles, as suggested in Yamamoto et al., 2003), smaller vesicles were detected throughout the cytoplasm (Figure 9A). In addition, plastids containing starch granules were frequently observed in wild-type pollen grains (Figures 9B and 9C). Figures 9D to 9F show that weakly affected mutant pollen still contained the vegetative nucleus, mitochondria, and even occasional lipid bodies. However, the plastid-like structures appeared to be free of starch granules (Figure 9F). Even in these weakly affected pollen grains, autolysis was obvious at several sites. In moderately affected pollen, autolysis was more extensive, and the organelles in the vegetative cell seemed to be clustered (Figures 9G and 9H), although distinguishable mitochondria and Golgi stacks were still present. Vacuole-like structures were observed only very rarely (Figure 9I). Large inclusions were detected in all mutant pollen grains (Figures 9D, 9G, and 9J). In strongly affected pollen, autolysis leads to the disintegration of basic structures (Figures 9J and 9K). This process was accompanied by a swelling of the intine wall and retraction of the plasma membrane (Figure 9L). Despite the severity of the damage in the vegetative cells, the exine layer of these pollen grains was still essentially wild-type (Figures 9C and 9L), as confirmed by scanning electron microscopy (Figure 6H).

The *gpt1* Lesion Arrests Embryo Sac Development

As outlined above, siliques of both the *GPT1/gpt1-2* and *GPT1/gpt1-1* lines contained ~30% aborted ovules (Table 4), and in

Table 3. Analysis of Genetic Transmission of *gpt1-1* and *gpt1-2*

Genotype (Female $\times$ Male)	Kan^r/PCR$^+$	Kan^s/PCR$^-$	TE (%)
GPT1/gpt1-1 $\times$ Ws-2	47	137	34
Ws-2 $\times$ *GPT1/gpt1-1*	26	128	20
GPT1/gpt1-2 $\times$ Ws-2	30	112	27
Ws-2 $\times$ *GPT1/gpt1-2*	28	142	20
GPT1/gpt1-2 $\times$ Col-0	13	36	36
Col-0 $\times$ *GPT1/gpt1-2*	11	45	24

The inheritance of *gpt1-1* was analyzed by counting kanamycin-resistant F1 progenies of the denoted crosses. The inheritance of *gpt1-2* was monitored using a PCR-based assay as described in Methods. The TE was calculated according to Howden et al. (1998). Kan^r, kanamycin resistant; Kan^s, kanamycin sensitive.

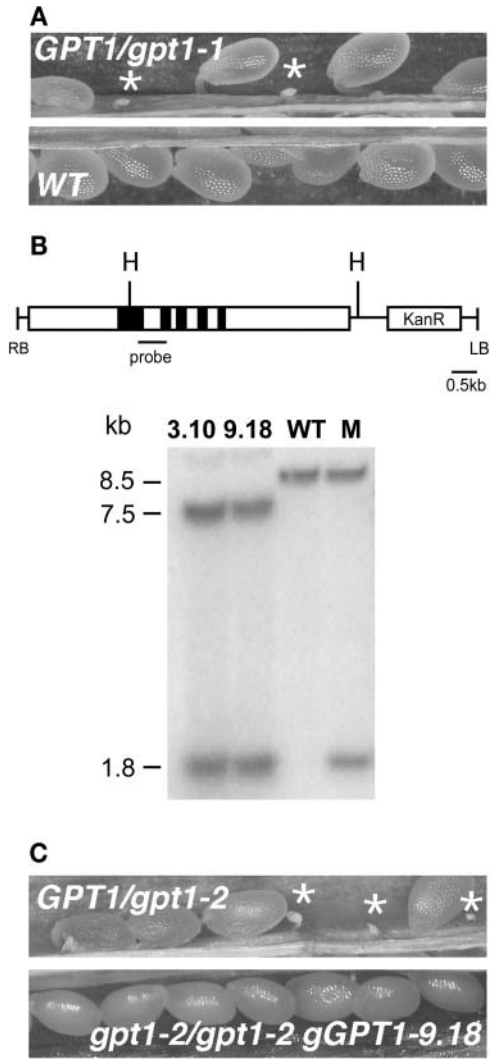

Figure 5. Seed Phenotype of *gpt1* Alleles and Genetic Complementation.

(A) Top panel: mature silique of a *GPT1/gpt1-1* plant. The asterisks denote aborted, white, and shrunken ovules. Bottom panel: mature silique of the wild type.

(B) Schematic representation of the genetic fragment used for complementation. DNA gel blot analysis of *Hin*dIII-digested DNA (10 μg) from two complemented lines, *gpt1-2 gGPT1-3.10* and *gpt1-2 gGPT1-9.18*, and comparison with the wild type and the *GPT1/gpt1-2* line. The probe used for hybridization is indicated. M, heterozygous mutant line; H, *Hin*dIII.

(C) Top panel: mature silique of a *GPT1/gpt1-2* plant. The asterisks denote aborted, white, and shrunken ovules. Bottom panel: mature silique of the T3 generation of the complemented line *gpt1-2/gpt1-2 gGPT1-9.18*. Note the absence of aborted ovules.

both lines, the TE of the *gpt1* allele was reduced. The actual frequency of aborted ovules is in good agreement with the value expected (average of 32%) on the basis of the transmission data (Table 3). Detection of *GPT1*:*uidA* expression within the embryo sac (Figure 10A) is compatible with a role for GPT1 during female gametophyte development. We therefore investigated the nuclear constitution of the embryo sacs in affected ovules 48 h after the emasculation of *GPT1/gpt1-2* flowers. In ovaries of wild-type plants, all embryo sacs reached the terminal developmental stage (containing one secondary nucleus, one egg cell nucleus, and two synergid cell nuclei). However, in ovaries of *GPT1/gpt1-2* plants, only 64% ($n = 117$) of embryo sacs displayed the wild-type phenotype (Figure 10B). The majority of mutant embryo sacs were consistently found to possess two slightly larger nuclei lying side by side and to display a variable number of smaller nuclei (Figure 10C). This phenotype resembles that of the *gfa2* mutant described by Christensen et al. (2002), in which the polar nuclei fail to fuse. In that study, the polar nuclei migrated properly, came to lie side by side, and were slightly enlarged. Thus, it is most likely that *gpt1* mutant embryo sacs are defective in nuclear fusion. A small fraction of the remaining embryo sacs was found to be in an advanced state of degeneration, containing only one nucleus (Figure 10D). After pollination, the two larger polar nuclei persisted in mutant embryo sacs until the stage at which the proembryo and the suspensor became distinguishable in wild-type seeds (data not shown).

GPT2 Function Is Not Essential for Gametogenesis

Although these data indicate that the GPT1 protein is essential for efficient gametophyte development, a fraction of the gametophytes still remains functional, indicating incomplete penetrance of the mutation. Therefore, the question arises whether GPT2 can partly substitute for GPT1. The expression data for GPT2 revealed low expression levels in stamens and carpels (Figure 2). However, no significant *GPT2* expression was found in uninuclear, bicellular, or tricellular pollen grains (data from the Nottingham Arabidopsis Stock Centre [NASC] at the Genevestigator Web site, https://www.genevestigator.ethz.ch/). Furthermore, a line was identified in the GABI-Kat collection (Li et al., 2003), which contained a T-DNA insertion at position +1433 relative to the start codon (*gpt2-1*). No *GPT2* transcripts are detectable in homozygous *gpt2-1* mutants by RT-PCR (data not shown). These lines exhibited essentially wild-type growth and development under greenhouse conditions (data not shown). Because a slight reduction in fertility might not have been detectable under these conditions, the mutant flowers were examined by microscopy for pollen and ovule aberrations. Neither the frequency of aborted pollen (0.4%, $n = 6400$), as revealed by the Alexander stain, nor that of aborted ovules (4%, $n = 716$) differed from that observed in the wild type. Together, the data suggest that the GPT2 function has only minor influence on pollen and embryo sac development.

DISCUSSION

In Planta Function of AtGPT1 and AtGPT2

The GPTs represent one of the four known subfamilies of plastidic phosphate translocators. The Arabidopsis genome contains two functional *GPT* genes, At*GPT1* and At*GPT2* (Knappe et al., 2003a), whose products share 75% sequence

identity. Both translocators show similar substrate specificities, accepting Glc6P and triose phosphates as countersubstrates for inorganic phosphate, and these specificities are similar to those of pea GPT (Table 1). The mode of GPT action is a 1:1 exchange of Glc6P mainly with inorganic phosphate and triose phosphates or an exchange of triose phosphates with inorganic phosphate (Kammerer et al., 1998). In addition, when ectopically expressed, both GPTs can rescue the low-starch leaf phenotype of the *pgi1* mutant, indicating that both proteins are able to deliver Glc6P to chloroplasts as a precursor for starch biosynthesis, thereby circumventing the necessity to convert Fru6P to Glc6P (the reaction catalyzed by PGI). Thus, both GPTs function as glucose-6-phosphate transporters in planta. However, their expression patterns differ markedly. Whereas *GPT1* is ubiquitously expressed, *GPT2* is expressed at a lower level in most tissues. Remarkably, *GPT2* is highly expressed in response to *Pseudomonas syringae* treatment (data not shown) and in a few tissues, such as senescing leaves (Figure 2). Whether AtGPT2 has a specific function during pathogen treatment and senescence remains to be determined. On the other hand, the expression pattern of At*GPT1* implies that it is the major GPT responsible for the transport of Glc6P into plastids of heterotrophic tissues in Arabidopsis. It is expressed in roots, as is the pea GPT (Borchert et al., 1993; Kammerer et al., 1998), and At*GPT1* expression is strongest in the root cap, the site of starch synthesis. In the *pgi1* mutant, starch synthesis in roots is not affected (Yu et al., 2000), most probably because Glc6P can be imported into amyloplasts via AtGPT1, thus bypassing the need for PGI. In leaves, At*GPT1* is expressed in guard cells and, to a lesser extent, also in mesophyll cells (Figures 3A to 3C). The expression in guard cells is in accordance with previous findings that guard cell chloroplasts lack fructose-1,6-bisphosphatase activity and therefore rely on the availability of hexose phosphate for starch

Table 4. Frequency of Aborted Ovules and Pollen in the Wild Type, *GPT1/gpt1-1*, *GPT1/gpt1-2*, and in Two Complemented Lines

Genotype	Normal Seed	Aborted Ovule[a]	Frequency (%)
GPT1/GPT1 (Ws-2)	755	53	6.6
GPT1/gpt1-1	507	236	32.0
GPT1/gpt1-2	1357	530	28.0
gpt1-2/gpt1-2 gGPT1-3.10	1461	104	6.6
gpt1-2/gpt1-2 gGPT1-9.18	1433	68	4.5
	Normal Pollen	Aborted Pollen[b]	
GPT1/GPT1 (Ws-2)	9343	75	0.8
GPT1/gpt1-1	3301	332	9.0
GPT1/gpt1-2	3242	581	15.0
gpt1-2/gpt1-2 gGPT1-3.10	10000	57	0.6
gpt1-2/gpt1-2 gGPT1-9.18	10000	87	0.9

[a] Aborted ovules were counted in the 10th to 12th siliques of the main inflorescence of the indicated genotype at a stage when the final silique size was reached.

[b] Aborted pollen were counted after Alexander staining of released pollen from the denoted genotype. In this assay, aborted pollen grains stain green.

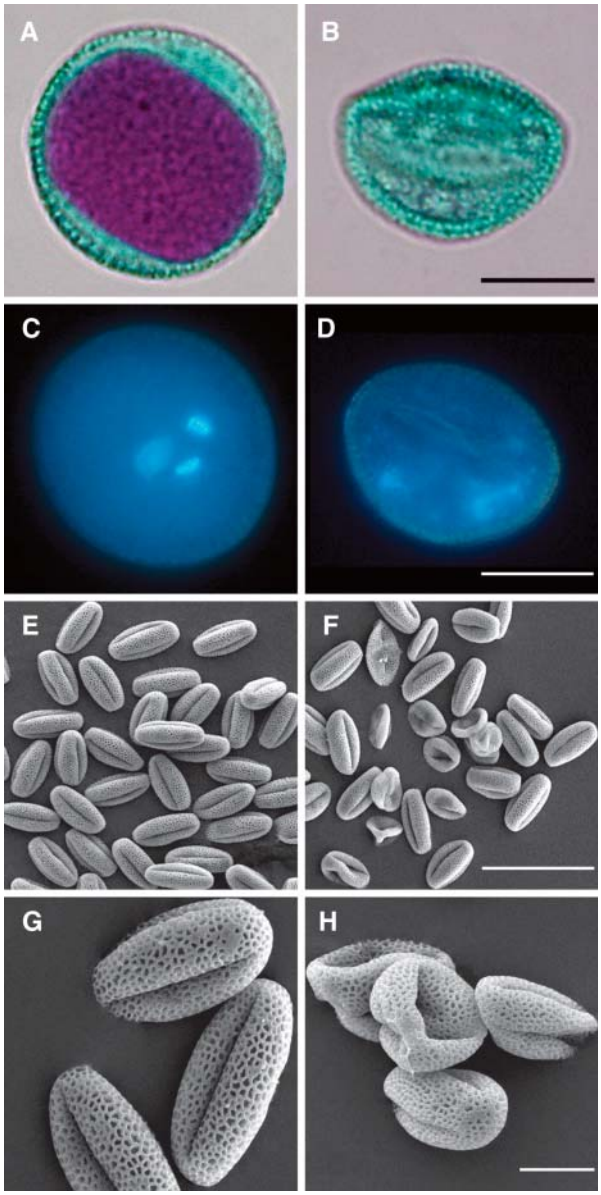

Figure 6. Loss of GPT1 Function Perturbs Pollen Development.

Pollen grains were released from the wild type and *GPT1/gpt1-2*. Similar observations were made with pollen released from *GPT/gpt1-1*.

(A) and **(B)** Bright-field image of whole-mount Alexander-stained pollen. The wild-type pollen shows intensive red staining in the cytoplasm **(A)**. Note the absence of red cytoplasmic staining in *gpt1* pollen **(B)**. Bar = 10 μm.

(C) and **(D)** Fluorescent image of whole-mount DAPI-stained pollen. The wild-type pollen shows two sperm nuclei and one centrally located vegetative nucleus **(C)**. Note the diffuse staining in *gpt1* pollen **(D)**. Bar = 10 μm.

(E) to **(H)** Scanning electron micrographs of mature pollen grains from wild-type (**[E]** and **[G]**) and *GPT1/gpt1-2* plants (**[F]** and **[H]**). Of the 28 pollen grains shown, 10 have an abnormal structure **(F)**. However, in the abnormal pollen grains, the exine structure is still intact **(H)**. Bar = 50 μm for **(E)** and **(F)** and 10 μm for **(G)** and **(H)**.

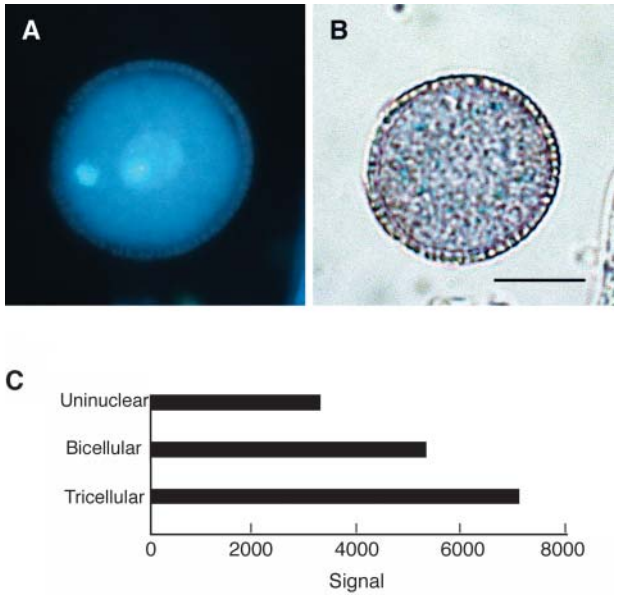

Figure 7. *GPT1* Expression in Pollen Grains.

GPT1 expression was analyzed in *GPT1*:*uidA* pollen and by making use of publicly available microarray data (Zimmermann et al., 2004).
(A) Fluorescent image of DAPI-stained tricellular pollen.
(B) Bright-field image of GUS activity in tricellular pollen. Because the GUS protein is fused to the N-terminal presequence of GPT1, the fusion protein is directed to plastids. Bar = 10 μm.
(C) Digital Northern of *GPT1* expression in uninuclear, bicellular, and tricellular pollen grains. Data used to create the Digital Northern were obtained from NASC at the Genevestigator site (https://www.genevestigator.ethz.ch/). Signal intensities were averaged from the two technical replicates.

biosynthesis (Hedrich et al., 1985). The subsequent breakdown of starch yields malate as a counter ion for potassium during stomatal opening. In contrast with mesophyll chloroplasts, envelope membranes of guard cell chloroplasts have been shown to have GPT transport activity (Overlach et al., 1993). The At*GPT1* expression observed in Arabidopsis leaf mesophyll cells is somewhat surprising because the chloroplasts of these cells do not depend on the import of reduced carbon sources and Glc6P transport activities are not detectable (data not shown). Also, the low-starch leaf phenotype of the *pgi1* mutant obviously cannot be compensated for by the endogenous AtGPT1 activity. It is conceivable that expression of *GPT1* mRNA in these cells serves as a standby system (i.e., that synthesis or activation of the GPT1 protein operates only on demand). This assumption is corroborated by the observation that, upon feeding with glucose, a specific Glc6P transport system is induced in spinach (*Spinacia oleracea*) leaves leading to starch accumulation (Quick et al., 1995).

AtGPT1 Is Crucial for Normal Male Gametogenesis

No obvious abnormalities could be detected in heterozygous *gpt1* lines; indeed, the mutation was expected to be recessive. However, the phenotypic and genetic analyses revealed a major role of *GPT1* in the haploid phase of Arabidopsis development, namely, during embryo sac and pollen development.

Given the apparent physiological role of GPT1—import of Glc6P into plastids—the question arises why a defect in Glc6P transport should cause such a severe phenotype as that observed in *gpt1* pollen. Glc6P that enters the plastid via the GPT1 can be used (1) as a carbon source for starch biosynthesis, (2) as a substrate for fatty acid biosynthesis, or (3) as a starter molecule for the OPPP. The role of GPT1 in delivering the precursor for starch biosynthesis is obvious because plastids harboring starch granules were frequently found in wild-type pollen grains (Figures 9B and 9C). By contrast, the mutant *gpt1* pollen only contained starch-free plastids (Figure 9F). However, the existence of

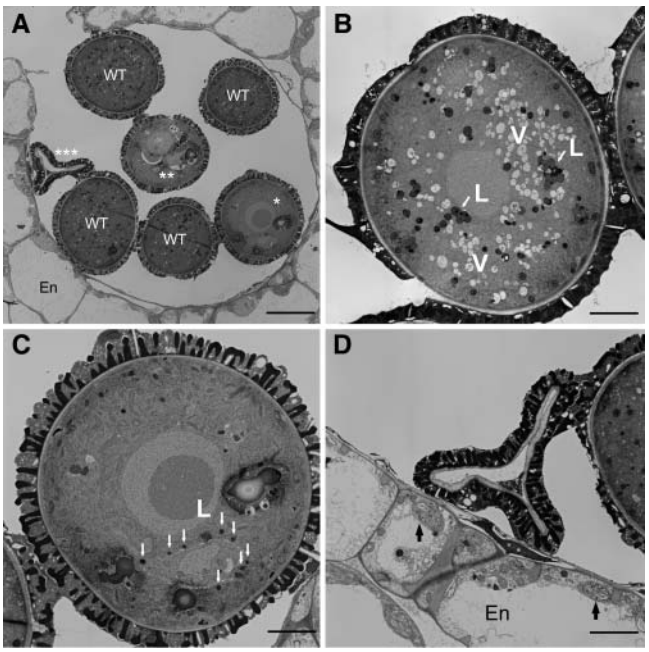

Figure 8. Pollen Sacs from *GPT1*/*gpt1-2* Plants Contain a Mixture of Normal and Mutant Pollen Grains.

Cross sections of pollen sacs from *GPT1*/*gpt1-2* anthers (stage 12) were analyzed using transmission electron microscopy. In anthers at stage 12 (according to Sanders et al., 1999), the tapetum und middle layers disintegrate, and the anthers become bilocular and contain tricellular pollen grains. En, endothecium cell; L, lipid bodies; V, vacuoles. Bar = 10 μm in **(A)** and 3 μm in **(B)** to **(D)**.
(A) Overview of a pollen sac. In addition to pollen grains with wild-type morphology, pollen grains displaying varying degrees of damage were present. The number of asterisks denotes the severity of damage.
(B) Cross section of a wild-type pollen grain. Note the occurrence of dispersed vacuoles and lipid bodies (arrows). Lipid bodies are darkly stained because osmium tetroxide was added during the fixation procedure.
(C) Cross section of a weakly affected mutant pollen grain. Note the absence of vacuoles and the reduced number of lipid bodies (arrows).
(D) Cross section of a collapsed pollen grain. The adjacent endothecial cells possessed plastids containing starch and plastoglobuli, as indicated by the arrows.

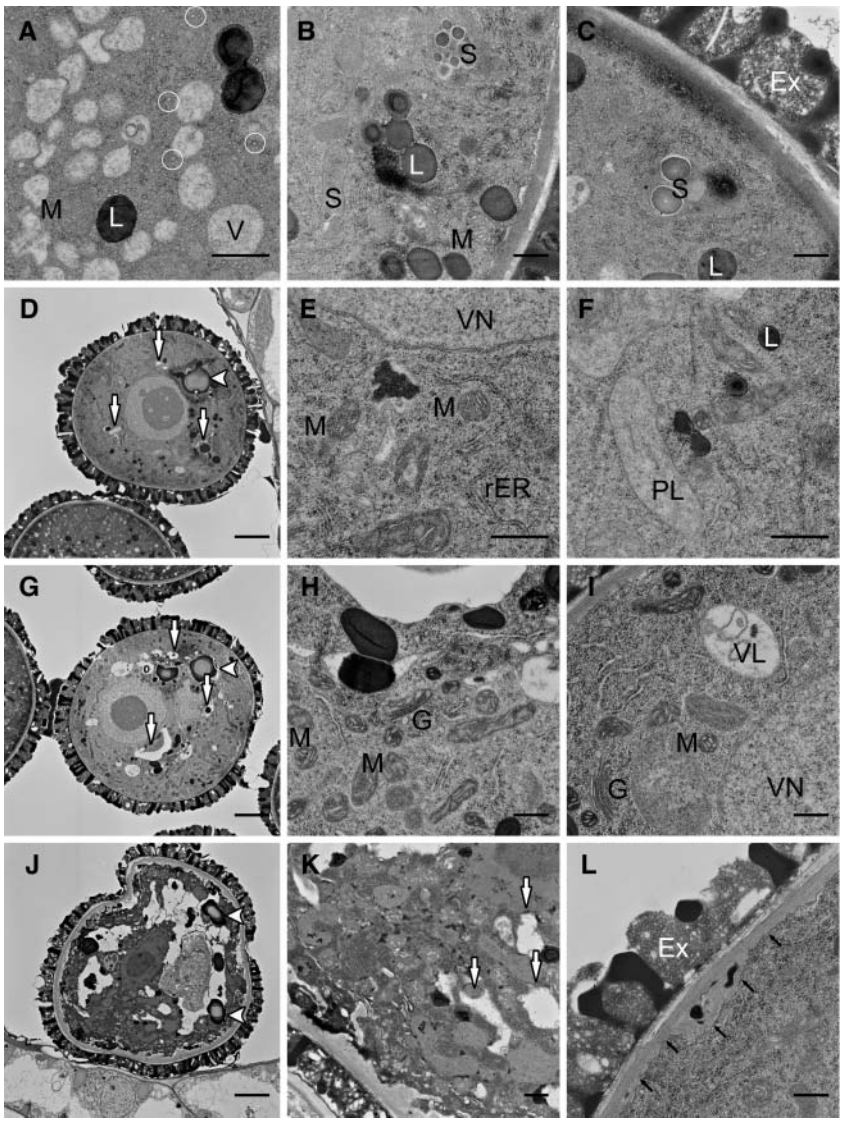

Figure 9. Ultrastructural Alterations in *gpt1* Mutant Pollen.

Cross sections of differently affected *gpt1* mutant pollen grains were analyzed using transmission electron microscopy when the corresponding wild-type pollen had reached the tricellular stage. M, mitochondria; L, lipid body; V, vacuole; S, starch granules within plastid; Ex, exine layer; VN, vegetative nucleus; PL, plastid-like structure; G, Golgi apparatus; VL, vacuole-like body. Bars = 0.75 μm in **(A)** to **(C)**, **(E)**, **(F)**, **(H)**, **(I)**, **(K)**, and **(L)** and 3 μm in **(D)**, **(G)**, and **(J)**.

(A) to **(C)** Details of a tricellular, mature wild-type pollen grain. Mitochondria, darkly stained lipid bodies, vacuoles, the starch granules within a plastid, and the exine layer are indicated. Some small vesicles are circled.

(D) Overview of a weakly affected mutant pollen grain. Autolysis has begun at several sites (arrows). A large inclusion is indicated by the arrowhead.

(E) Detail of the weakly affected mutant pollen grain shown in **(D)**. Mitochondria, the rough ER, and the vegetative nucleus are indicated.

(F) Detail of a weakly affected mutant pollen (comparable to that shown in **[D]**). The lipid body is indicated. Note that the plastid-like structure, which is similar in size to wild-type plastids, is surrounded by two membranes but lacks starch granules.

(G) Overview of a moderately affected mutant pollen grain. Zones of autolysis extend from several sites (indicated by the arrows). A large inclusion is indicated by the arrowhead.

(H) Detail of the moderately affected mutant pollen grain shown in **(G)**. Mitochondria and part of the Golgi apparatus are indicated.

(I) Detail of a moderately affected mutant pollen grain (comparable to that in **[G]**). Note the occurrence of a vacuole-like structure. Vegetative nucleus, Golgi apparatus, and mitochondria are indicated.

(J) Overview of a strongly affected mutant pollen grain. Autolysis involves nearly half of the pollen grain. Two large inclusions are indicated by arrowheads.

(K) Detail of the strongly affected mutant pollen grain shown in **(J)**. Internal structures are no longer distinguishable; sites of autolysis are indicated by arrows.

(L) Detail of a strongly affected mutant pollen grain (comparable to that shown in **[J]**). The exine layer is similar to the wild-type pollen coat. Swelling of the pollen intine wall and recession of the plasmalemma are indicated by arrows.

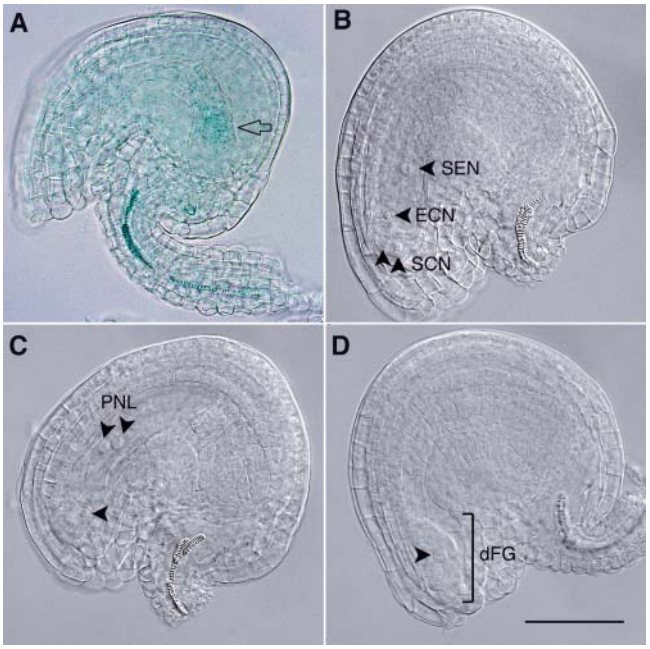

Figure 10. *GPT1*:*uidA* Expression in Ovules and the Terminal Developmental Stage of *gpt1-2* Embryo Sacs.

(A) Bright-field image of GUS activity in *GPT1*:*uidA* ovules. The plane of focus is on the chalazal region of the ovule, and the embryo sac is indicated by an arrow.

(B) to **(D)** Examination of the terminal developmental stage of *gpt1-2* embryo sacs. Flowers of *GPT1*/*gpt1-2* plants were emasculated, and whole-mount preparations of ovules were analyzed by differential interference contrast (DIC) microscopy 48 h after emasculation.

(B) DIC image of an ovule harboring a wild-type embryo sac. The wild-type embryo sac is at the terminal developmental stage, comprising one secondary nucleus, one egg cell nucleus, and two synergid cell nuclei at the micropylar end (indicated by arrowheads). SEN, secondary nucleus; ECN, egg cell nucleus; SCN, synergid cell nuclei.

(C) DIC image of an ovule harboring a mutant embryo sac. In the mutant embryo sac, two slightly enlarged nuclei lie side by side. These two nuclei resemble polar nuclei before fusion and are termed polar nuclei like. One additional smaller nucleus is also visible (indicated by an arrowhead). PNL, polar nuclei like.

(D) DIC image of an ovule harboring a degenerating embryo sac. The mutant embryo sac has collapsed and contains only one nucleus (indicated by the arrowhead). dFG, degenerating female gametophyte. Bar = 50 μm.

several starch-free mutants of Arabidopsis (Lin et al., 1988; Kofler et al., 2000) that retain full fertility and display no reduction in pollen viability (P. Niewiadomski and A. Schneider, unpublished results) demonstrates that starch accumulation per se is not a prerequisite for pollen development.

Glc6P or even triose phosphates can also be used as a carbon skeleton for fatty acid biosynthesis. However, fatty acid biosynthesis also can be driven by a range of alternative substrates (e.g., phospho*enol*pyruvate, acetate, malate, or pyruvate) (for review, see Fischer and Weber, 2002). Therefore, it remains unclear to what extent Glc6P and triose phosphates might serve as precursors for fatty acid biosynthesis. Nevertheless, we assume that GPT1 fulfils an essential role in fatty acid metabolism during pollen development. Fatty acid biosynthesis in the plastids depends on the availability of reducing equivalents, which are generated by the first enzymatic reactions in the OPPP. An inadequate supply of Glc6P as a precursor for the OPPP, therefore, would restrict activity of the fatty acid synthase complex. It has been shown that a mutation in enoyl-ACP reductase, which catalyzes the final reaction in the de novo fatty acid biosynthesis cycle and consumes reducing equivalents, leads to premature cell death and altered morphology in Arabidopsis (Mou et al., 2000). Although the *mod1* mutation, a single amino acid substitution in the enoyl-ACP reductase, allowed residual enzyme activity and caused a reduction of only ~10% in lipid content, the pleiotropic morphological effects in this mutant were severe (Mou et al., 2000). A role for GPT1 in fatty acid metabolism during pollen development is supported by the following observations: *GPT1* expression increases during pollen development (Figure 7), as one would expect if the GPT1 function has to meet increasing demands for reducing equivalents for fatty acid biosynthesis. In developing pollen grains, oil body accumulation, as well as the proliferation of an extensive network of endoplasmic reticulum (ER) membranes and vesicles, have been reported to commence after the first pollen mitosis (Piffanelli et al., 1998) Likewise, the pattern of lipid marker gene expression coincides with the accumulation of intracellular storage and membrane lipid components in *Brassica napus* pollen (Piffanelli et al., 1997). Furthermore, while weakly affected *gpt1* pollen grains still possessed lipid bodies, the overall number of lipid bodies in mutant pollen was significantly reduced. The variation in lipid body content and in pollen viability might be caused by variable rates of GPT1 protein depletion, with functional GPT1 protein presumably being carried over from plastids of the microspore mother cell. There was no indication for the involvement of *GPT2*, although the possibility that *GPT2* is activated in the absence of *GPT1* cannot be excluded.

A defect in lipid biosynthesis should also affect the integrity of cell membranes. The membrane-bound glycerol-3-phosphate acyltransferase (GPAT) mediates the initial step in glycerolipid biosynthesis in extraplastidic compartments of plant cells. The Arabidopsis *gpat1* mutant displays defects in ER membrane biogenesis and altered oil body size in pollen grains; *gpat1* pollen grains, moreover, show reduced competitiveness in fertilization (Zheng et al., 2003). Surprisingly, in weakly and moderately affected *gpt1* pollen, the ER network and other membrane systems, like the nuclear membrane, the Golgi apparatus, and mitochondria, were not visibly altered compared with the wild type. Only in strongly affected *gpt1* pollen grains was a disorganization of the plasma membrane observed. This phenomenon, however, may be considered as a secondary effect because it was associated with a swelling of the pollen wall and occurred only at an advanced state of autolysis.

Another striking feature of *gpt1* mutant pollen was the almost complete absence of dispersed vacuoles in tricellular pollen (Figures 8C and 9D to 9L). In the wild type, the vacuoles undergo serial transformations during pollen development (e.g., in microspores, a large vacuole appears, which divides into small vegetative vacuoles after the first mitosis) (Yamamoto et al., 2003). These vegetative vacuoles disappear after the second

Table 5. Expression Analysis of Genes Involved in Plastidic OPPP Metabolism

	Pollen Expression		
Gene Number	Uninuclear	Bicellular	Tricellular
G6PDH genes:			
At1g09420	503	540	359
At1g24280	1432	1340	537
At5g13110	3094	3192	1033
At5g35790	221	223	72
6PGDH genes:			
At1g64190	2511	2567	205
At3g02360	12306	15145	21713

Genes encoding plastidic isoforms are listed (Kruger and von Schaewen, 2003). Data represent signal intensities averaged from two technical replicates and were obtained from the NASC at the Genevestigator site (https://www.genevestigator.ethz.ch/). Note that expression of *GPT1* is markedly increased in tricellular pollen grains (see Figure 7C).

mitosis, and in mature pollen grains, storage vacuoles appear that are produced de novo from the rough ER. Finally, in pollen grains from flowers in bloom, these storage vacuoles are converted into lytic vacuoles (Yamamoto et al., 2003). In all microspores of heterozygous *gpt1* plants, the large vacuole was intact (data not shown). In tricellular *gpt1* pollen grains, however, vacuoles were nearly completely absent (Figures 8C and 9D to 9I). The absence of vacuoles in *gpt1* pollen might be explained as a direct consequence of reduced fatty acid biosynthesis, which will lead to a relative lack of components for the formation of the vacuole membranes. Interestingly, a mutation in the *VCL1* gene, which is essential for vacuole biogenesis, affects pollen performance after germination, yet it is not lethal in the gametophyte (Hicks et al., 2004).

In summary, we propose the following working model for the function of GPT1 in pollen development: Developing pollen has a high demand for fatty acids. In *gpt1* pollen, lack of Glc6P results in a reduced supply of reducing equivalents via the OPPP, which directly affects the formation of lipid bodies and vacuoles. The decrease in the level of lipid bodies and of vacuoles is not lethal per se, but the vegetative cell may sense the severe impairment of fatty acid biosynthesis and might initiate an autolytic process leading to nonphysiological cell death. This model is in accordance with the finding that interruption of any vital metabolic process inevitably leads to nonphysiological cell death (Vaux and Korsmeyer, 1999). The model is also supported by the observation that the onset of autolysis precedes the disintegration of mitochondria, rough ER, Golgi stacks, and nuclear membranes (Figures 9D and 9G).

Reducing equivalents are generated via the OPPP in reactions catalyzed by glucose-6-phosphate 1-dehydrogenase (G6PDH; EC 1.1.1.49) and 6-phoshogluconate dehydrogenase (6PGDH; EC 1.1.1.44). In the case that the OPPP plays a pivotal role during pollen development, genes encoding these enzymes should be expressed in these tissues. The expression pattern of genes, which are likely to encode plastidic isoforms of G6PDH and 6PGDH (Kruger and von Schaewen, 2003) are summarized in Table 5. Of the four genes coding for G6PDH and the two genes coding for 6PGDH, the expression pattern of the *6PGDH* gene *At3g02360* closely resembled that of *GPT1* (i.e., highest expression was found in tricellular pollen grains). In addition, an insertion mutant of this gene (*At3g02360*) produced a high number (32%) of aborted pollen and could not be established in the homozygous state, as is the case for *gpt1* (P. Niewiadomski and A. Schneider, unpublished results). This indicates that the product of *At3g02360* might be crucial for both the OPPP and pollen development, suggesting a functional relationship between the oxidative part of the OPPP and pollen development.

Involvement of AtGPT1 in Embryo Sac and Seed Development

In addition to its essential role during pollen maturation, GPT1 is important for normal embryo sac development. Thus, the *gpt1* mutation affected the fusion of the polar nuclei during embryo sac development (Figure 10C). In the wild type, fusion of the polar nuclei involves fusion of outer and inner nuclear membranes, and the fusion of the outer nuclear membrane has been suggested to be dependent on the mitochondrial GFA2 protein (Christensen

Table 6. Primers Used in This Study

Primer Name	Primer Sequence
GPT1PromF	5′-CTCATTTGAATTCTTCTTAG-3′
GPT1PromR	5′-CGCAGGTTCACCACTCTTGAT-3′
GPT2-F1	5′-CACCTCGAGATCATAGTC-3′
GPT2-R1	5′-CACCGGAATGTTCTCTCCTCC-3′
F-LB	5′-GATGCACTCGAAATCAGCCAATTTTAGAC-3′
F-RB	5′-TCCTTCAATCGTTGCGGTTCTGTCAGTTC-3′
JL-202	5′-CATTTTATAATAACGCTGCGGACATCTAC-3′
S-LB	5′-GTCCGCAATGTGTTATTAAGTTGTC-3′
GK-LB	5′-ATATTGACCATCATACTCATTGC-3′
GPT1-Fw	5′-GCCATGAAAGTAAAATATTCACGCTAAAG-3′
GPT1-F1	5′-TCACGCTAAAGAGAAATTG-3′
GPT2-F2	5′-GTCGGACCAAACTTTGTCTGGT-3′
GPT1-F3	5′-GCATTCTTGTCCTGTTCCTAG-3′
GPT1-F4	5′-ACCCACATGATGAGACTTAAG-3′
GPT1-F5	5′-TGTCTTAATTACATTTCAAGA-3′
GPT1-F6	5′-AGAACAGCATCCTAGAATTCCAAAAATGA-3′
GPT1-R1	5′-ATCTGTTTGTACTTTACTTCTCTCTGGTC-3′
GPT1-R2	5′- TCCTTCACCAAACATATCTCTC-3′
GPT1-R3	5′-GGTATTTTGGTCAAGGTAAGG-3′
GPT1-R4	5′-ATCATCACCGATCGGATGAG-3′
GPT1-R5	5′-GTGTGTGCCACAGCAACCTATATGCA-3′
GPT1-R6	5′-GGTTTTGGTTTACTTTCAGTTGG-3′
GPT1-R7	5′-TCAAGGTAAGGTTATGTTTACCTGGGAAT-3′
GPT2-F2	5′-GTCGGACCAAACTTTGTCTGGT-3′
GPT2-R2	5′-GGTCTGATCAAGAAATGACACTGA-3′
AtACT2/8fwd	5′-GGTGATGGTGTGTCT-3′
AtACT2/8rev	5′-ACTGAGCACAATGTTAC-3′
GPT1RT-F	5′-TGGCTTACCTCGACGCTTTCT-3′
GPT1RT-R	5′-TACTCACCGTTGCAGCCACAT-3′
GPT2RT-F	5′-CTTCGAATTTCAAGCGTGAGG-3′
GPT2RT-R	5′-TCTGCGCGGATTGTTCATC-3′

Primers were used for the identification and verification of *gpt1* and *gpt2* mutants, for the generation of constructs, and for RT-PCR analysis.

et al., 2002). Although it is premature to speculate on the underlying mechanism, At*GPT1* clearly also has a gametophytic effect on female fertility. An involvement of the OPPP seems possible because plastids of the female gametophyte might also depend on the import of reduced carbon sources via GPT1 for the generation of reducing equivalents.

Furthermore, although 5 to 9% homozygous *gpt1* lines are predicted based on TEs measured, we never recovered a homozygous adult plant. Therefore, future work will involve the generation of lines in which the gametophytic defects of the *gpt1* mutation are removed (e.g., by complementing the *gpt1* mutant with *GPT1* driven by a pollen-specific and/or embryo sac–specific promoter). This would allow us to investigate the effects of loss of GPT1 function in the sporophyte, in particular during seed development. It is worth noting that *GPT*:*uidA*-based (see Figures 3G to 3L) and microarray-based analyses have shown that the expression of *GPT1* in seeds covaries with the one of starch metabolizing enzymes (Ruuska et al., 2002). Therefore, it will be interesting to see if GPT1 plays a role during the starch accumulating phase and/or during the oil accumulating phase throughout embryogenesis.

METHODS

Plant Material

Seeds of *Arabidopsis thaliana* (Heynh.) (ecotypes Ws-2 [N1601] and Col-0 [N1093], a collection of 6500 T-DNA–transformed lines obtained by seed transformation [Feldmann collection; Forsthoefel et al., 1992] and arranged in pool sizes of 100 [N3115 and N6500] and 20 [N3116 and N6400], and two lines identified at the Salk Institute [N521762 and N589293]) were provided by the NASC (http://nasc.nott.ac.uk/home.html). Seeds of pools 2, D, plate 66 and 8, F, plate 67 were obtained from the AKF (http://www.biotech.wisc.edu/Arabidopsis/), and seeds of line 454A06 were supplied by GABI-Kat (http://www.mpiz-koeln.mpg.de/GABI-Kat/). Plants were grown in a temperature-controlled greenhouse in a light/dark cycle of 16 h/8 h or in a growth chamber in a light/dark cycle of 12 h/12 h at day/night temperatures of 21°C/18°C and 40% humidity.

Construction of Promoter:*uidA* and 35S:cDNA Fusions and Analysis of Transgenic Plants

The GPT1-promoter-GUS construct was generated as a translational fusion by ligating a DNA fragment comprising the promoter and the 5′ end of the coding region of *GPT1* to the *uidA* gene. The AtGPT1 DNA fragment (2.1 kb) was generated using a proofreading DNA polymerase (Pfx; Invitrogen, Karslruhe, Germany) and the primer combination GPT1PromF/GPT1PromR (for primer sequences, see Table 6) and subcloned into pBluescript KS− (pBS; Stratagene, La Jolla, CA). After restriction with *Sal*I/fill in-*Xba*I, the DNA fragment was cloned into *Sma*I+*Xba*I-digested pGPTV-bar vector (Becker et al., 1992), resulting in pGPT1prom. The 35S:cDNA constructs were assembled starting from the appropriate cDNAs. The AtGPT1 cDNA was identified by screening an Arabidopsis cDNA library (Clontech, Palo Alto, CA) and subsequently subcloned into pBS (Stratagene) to give pGPT1. The AtGPT2 cDNA was amplified by RT-PCR using the gene-specific primers GPT2-F1/GPT2-R1 (Table 6) and subcloned into pGEM-T*easy* (Promega, Madison, WI), resulting in pGPT2. The 35S:GPT constructs were generated by cloning the *Sac*II/fill in-*Sal*I fragments of pGPT1 and pGPT2 into the *Sma*I+*Sal*I-digested pBinAR-Kan vector (Höfgen and Willmitzer, 1990), resulting in p35SAtGPT1 and p35SAtGPT2, respectively. The 35S:PsGPT construct was generated by cloning the *Sma*I-*Sal*I fragment of PsGPT-cDNA (Kammerer et al., 1998) into the *Sma*I+*Sal*I-digested pBinAR-Kan, resulting in p35SPsGPT. Transgenic plants were generated by vacuum infiltration of Arabidopsis plants using *Agrobacterium tumefaciens* cultures containing the appropriate construct (Bechtold et al., 1993). The primary transformants were allowed to flower and produce seeds.

Transformants were selected with BASTA or kanamycin and verified by PCR analysis. Histochemical localization of GUS in transgenic plants harboring the *GPT1*:*uidA* construct was performed as described previously (Knappe et al., 2003b). The starch content of leaves from control plants and transgenics harboring 35S:cDNA constructs was determined by the method described by Lin et al. (1988).

Isolation of *gpt1* and *gpt2* Alleles

The Feldmann collection was subjected to PCR using primers F-LB, F-RB, and GPT1-R5 (for primer sequences, see Table 6) as described previously (Schneider et al., 2002). The AKF BASTA population was screened for *gpt1* insertion alleles using a primer specific for the T-DNA left border (JL-202) in combination with GPT1-Fw (see http://www.biotech.wisc.edu/arabidopsis for Methods). Appropriate PCR bands were identified by DNA gel blot analysis using the AtGPT1 cDNA as a probe, subcloned, and sequenced. In silico analysis of the SALK and GABI-Kat databases (http://signal.salk.edu/cgi-bin/tdnaexpress and http://www.mpiz-koeln.mpg.de/GABI-Kat/) led to the identification of a *gpt2* and additional *gpt1* insertion lines.

Genotyping of lines was done using a PCR-based approach. Genomic DNA was isolated (Liu et al., 1995) from each plant analyzed and used as a template for PCR amplification of DNA fragments corresponding to the wild-type alleles and the insertion alleles. For heterozygous lines, the following primer combinations were used: for the *gpt1-1* line, F-RB/GPT1-R5 and GPT1-F2/GPT1-R5; for the *gpt1-2* line, JI-202/GPT1-F3 and GPT1-F3/GPT1-R3, and for the *gpt1-4* line, S-LB/GPT1-R2 and GPT1-R2/GPT1-F3 (see Figure 4B; for primer sequences, see Table 6). For the homozygous *gpt1-3* line, S-LB/GPT1-F5 and GPT1-F2/GPT1-R4 were used, for *gpt1-5*, F-LB/GPT1-R4 and GPT1-F1/GPT1-R6, and for *gpt1-6*, JI-202/GPT1-F4 and GPT1-F4/GPT1-R1 (see Figure 4B, Table 6). The *gpt2-1* line (GABI-Kat line 454A06) was genotyped using the GPT2-specific primer combination GPT2-F2/GPT2-R2 and the T-DNA–specific primer GK-LB together with GPT2-R2. DNA gel blots (10 μg of DNA) were prepared and analyzed following standard protocols (Sambrook et al., 1989) using a 645-bp GPT1, a 708-bp RB, or a 299-bp LB fragment as the probe (Figure 4C).

Genetic Analysis

To examine gametophytic transmission of the *gpt1-1* (background Ws-2) and *gpt1-2* (background Ws-2) alleles, reciprocal test crosses were performed between wild-type (Ws-2 and Col-0) and mutant lines. Seeds harvested from crosses of *gpt1-1* with Ws-2 were sown on kanamycin-containing plates, and the resistance phenotype was scored. Seeds obtained from crosses of *gpt1-2* with Ws-2 or Col-0 were sown on soil, and genomic DNAs from the F1 progeny were analyzed by PCR using the primer combination JI-202/GPT1-F3. The success of crosses between *gpt1-2* and Col-0 was monitored using the cleaved-amplified polymorphic sequence marker ER (http://www.arabidopsis.org/; Konieczny and Ausubel, 1993). No cases of adventitious self-fertilization were detected among the F1 progeny. The TE of T-DNA via each type of gamete (TE male and TE female) was calculated as described previously (Howden et al., 1998). The percentage of arrested gametophytes based on transmission

data was calculated according to the following formula: (100 − background)/2 – TE × (100 – background)/2 = % aborting events.

Phenotypic Analysis and Quantification

Seed development was analyzed in the 10th to 12th siliques of the main inflorescence of self-pollinated heterozygous *gpt1* plants and wild-type plants at a stage when the final silique size had been reached. To determine the terminal phenotype of mutant ovules, flowers were emasculated and the ovule phenotype was analyzed 48 h after emasculation. Flowers were fixed for 16 h in an ethanol:acetic acid mixture (9:1), washed in 80 and 70% ethanol, and cleared in chloral hydrate:H_2O:glycerol (8:3:1).

Analysis of mature pollen with DAPI was performed as previously described (Park et al., 1998) Alexander staining of pollen was performed on released pollen grains by adding them directly to Alexander's stain (Alexander, 1969).

Preparations were examined with a light microscope (Eclipse E800; Nikon, Tokyo, Japan) equipped for differential interference contrast and fluorescence microscopy. Images were captured using a 1-CCD color video camera (KY-F1030; JVC, Singapore) operated by the DISKUS software package (Technisches Büro Hilgers, Königswinter, Germany).

Transmission and Scanning Electron Microscopy

Stamens for transmisssion electron microscopy were taken from different flower stages and fixed with 2% glutaraldehyde in 50 mM phosphate buffer, pH 7.4, overnight at 4°C. Samples were postfixed in 1% osmium tetroxide for 8 h on ice, dehydrated in a graduated acetone series, including a step with 1% uranylacetate (in 50% acetone, 2 h), embedded in Spurr's resin, and polymerized at 50°C for ~72 h. Ultrathin sections (60 to 70 nm) were cut with a diamond knife (Micro Star, Huntsville, TX) on a Leica Ultracut UCT microtome (Leica Microsystems, Vienna, Austria) and mounted on pioloform-coated copper grids. The sections were stained with lead citrate and uranyl acetate (Reynolds, 1963) and viewed with a Zeiss EM 109 transmission electron microscope (Carl Zeiss, Oberkochen, Germany) at 80 kV. Micrographs were taken using SO-163 EM film (Kodak, Rochester, NY).

For scanning electron microscopy, released pollen grains were mounted on stubs and sputter-coated with gold particles (S150A; Edwards, Crawley, UK). Specimens were examined with a scanning electron microscope (XL 30 ESEM; Philips, Eindhoven, The Netherlands) at an accelerating voltage of 15 kV.

Genetic Complementation

A genomic library of Arabidopsis in λEMBL3 (Clontech) was screened by plaque hybridization using the *AtGPT1* cDNA insert as a probe following standard protocols (Sambrook et al., 1989). A genomic DNA clone containing the *GPT1* locus was isolated and an 11-kb *Sal*I-*Bam*HI fragment was subcloned into pBS (Stratagene) and sequenced. The *Sal*I-*Bam*HI fragment, including the *GPT1* coding region flanked by 3.3 kb of 5′ and 5.3 kb of 3′ noncoding sequence, was excised from the cloning vector and inserted into the binary vector pGreen (Hellens et al., 2000), resulting in pGreen-GPT1. pGreen-GPT1 was introduced into *A. tumefaciens* strain 3101 containing pSoup (Hellens et al., 2000) and subsequently transformed into *GPT1*/*gpt1-2* plants (see Figure 5). Transgenic Arabidopsis plants were selected for kanamycin resistance. Segregation analysis of the endogenous *GPT1* locus was performed by PCR using the primer combination GPT1-F6/GPT1-R7 (Table 6) and TaKaRa Ex-*Taq* polymerase according to the manufacturer's instructions (BioWhittaker, Verviers, Belgium). Generation of a 5-kb fragment indicates the presence of the endogenous *GPT1* locus and not the introduced genomic *GPT1* fragment.

Expression Analysis

Total RNA was isolated from different mutant lines as previously described (Eggermont et al., 1996). Oligo(dT)-primed cDNA from 2 μg of total RNA (DNase treated) was synthesized using the SuperScript reverse transcriptase system (Invitrogen). Primers used for amplification were GPT1RT-F/GPT1RT-R and GPT2RT-F/GPT2RT-R (for primer sequences, see Table 6), and reactions were performed for 5 min at 95°C followed by 40 cycles of 30 s at 94°C, 1 min at 55°C, and 2 min at 72°C.

For the isolation of guard cell and mesophyll cell protoplasts, epidermal peels and epidermis-free developed rosette leaves were incubated for 2 h or 20 to 30 min, respectively, in solutions containing 0.8% (w/v) cellulase (Onozuka R-10; Serva, Heidelberg, Germany), 0.1% pectolyase (Sigma-Aldrich, St. Louis, MO), 0.5% BSA, 0.5% polyvinylpyrrolidone, 1 mM $CaCl_2$, and 10 mM Mes/Tris, pH 5.6. The osmolarity of the enzyme solution was adjusted to 540 (for guard cell protoplasts) or 400 (for mesophyll cell protoplasts) mosmol kg^{-1} with D-sorbitol. Protoplasts released from guard cells or mesophyll tissues were recovered by filtration through a 20-μm nylon mesh and washed twice in 1 mM $CaCl_2$ buffer. Protoplast RNA was purified twice with the Dynabeads mRNA Direct kit (Dynal, Oslo, Norway) to minimize DNA contamination. Quantitative real-time RT-PCR was performed in a Light Cycler (Roche, Mannheim, Germany) as described before (Ivashikina et al., 2003) using AtACT2/8fwd/AtACT2/8rev and GPT1RT-F/GPT1RT-R as primer pairs (for primer sequences, see Table 6).

In silico expression analysis was performed at https://www.genevestigator.ethz.ch/.

Heterologous Expression of AtGPTs in Yeast Cells and Reconstitution of Transport Activities

For heterologous expression in yeast cells, cDNAs coding for the mature forms of AtGPT1 and AtGPT2 were cloned into the yeast expression vector pYES2-NT (Invitrogen). The mature AtGPT1 was obtained by cloning the *Pvu*I/blunted-*Eco*RI fragment of pGPT1 into *Bam*HI/fill-in+*Eco*RI-digested pYES2-NTC, resulting in pYESmGPT1. The mature form of AtGPT2 was obtained by cloning the *Pvu*I/blunted-*Eco*RI fragment of pGPT2 into *Bam*HI/fill-in+*Eco*RI-digested pYES2-NTA, resulting in pYESmGPT2. Both constructs were transformed into the *Saccharomyces cerevisiae* strain INVSc1 (Invitrogen), and transformants were selected using *URA3* as the selective marker. The induction of protein expression was done according to the manufacturer's instructions. Yeast cells were harvested 6 h after induction and disrupted in 10 mM Tris-HCl, pH 7.5, 1 mM EDTA, and 300 μg mL^{-1} phenylmethylsulfonylfluoride. The 100,000*g* yeast membrane fractions were prepared by ultracentrifugation and solubilized using 2% (w/v) *n*-dodecyl maltoside, and the recombinant His6-GPT1 and His6-GPT2 proteins were then purified via metal affinity chromatography on Ni^{2+}-nitrilotriacetic acid agarose (Qiagen, Hilden, Germany) and used for reconstitution of transport activities. Reconstitution of whole tissue extracts and of transport activities was performed as previously described (Loddenkötter et al., 1993; Kammerer et al., 1998; Knappe et al., 2003b).

ACKNOWLEDGMENTS

We thank the Genomic Analysis Laboratory of the Salk Institute for providing the sequence-indexed Arabidopsis T-DNA insertion mutants, Kerstin Kunze, Hildegard Voll, Rita Grotjahn, and Barbara Hess for technical assistance, Siegfried Werth for photographs, Rita Gross-Hardt (University of Zürich, Switzerland) for support with ovule analysis, and Dario Leister (Max-Planck-Institute for Plant Breeding, Cologne,

Germany), Paul Hardy (University of Düsseldorf, Germany), and Eric van der Graaff for critical reading of the manuscript. This work was supported by grants from the Deutsche Forschungsgemeinschaft, the Bundesministerium für Bildung und Forschung, and the Fonds der Chemischen Industrie.

Received November 5, 2004; accepted January 13, 2005.

REFERENCES

Alexander, M.P. (1969). Differential staining of aborted and nonaborted pollen. Stain Technol. **44,** 117–122.

Alonso, J.M., et al. (2003). Genome-wide insertional mutagenesis of *Arabidopsis thaliana*. Science **301,** 653–657.

Baud, S., Guyon, V., Kronenberger, J., Wuilleme, S., Miquel, M., Caboche, M., Lepiniec, L., and Rochat, C. (2003). Multifunctional acetyl-CoA carboxylase 1 is essential for very long chain fatty acid elongation and embryo development in Arabidopsis. Plant J. **33,** 75–86.

Bechtold, N., Ellis, J., and Pelletier, G. (1993). *In planta Agrobacterium* mediated gene transfer by infiltration of adult *Arabidopsis thaliana* plants. C. R. Acad. Sci. **316,** 1194–1199.

Becker, D., Kemper, E., Schell, J., and Masterson, R. (1992). New plant binary vectors with selectable markers located proximal to the left T-DNA border. Plant Mol. Biol. **20,** 1195–1197.

Beckles, D.M., Smith, A.M., and ap Rees, T.A. (2001). A cytosolic ADP-glucose pyrophosphorylase is a feature of graminaceous endosperms, but not of other starch-storing organs. Plant Physiol. **125,** 818–827.

Borchert, S., Harborth, J., Schünemann, D., Hoferichter, P., and Heldt, H.W. (1993). Studies of the enzymic capacities and transport properties of pea root plastids. Plant Physiol. **101,** 303–312.

Bowsher, C.G., Boulton, E.L., Rose, J., Nayagam, S., and Emes, M.J. (1992). Reductant for glutamate synthase is generated by the oxidative pentose-phosphate pathway in nonphotosynthetic root plastids. Plant J. **2,** 893–898.

Carlsson, A.S., LaBrie, S.T., Kinney, A.J., von Wettstein-Knowles, P., and Browse, J. (2002). A KAS2 cDNA complements the phenotypes of the Arabidopsis fab1 mutant that differs in a single residue bordering the substrate binding pocket. Plant J. **29,** 761–770.

Caspar, T., Huber, S.C., and Somerville, C. (1985). Alterations in growth, photosynthesis, and respiration in a starchless mutant of *Arabidopsis thaliana* (L.) deficient in chloroplast phosphoglucomutase activity. Plant Physiol. **79,** 11–17.

Christensen, C.A., Gorsich, S.W., Brown, R.H., Jones, L.G., Brown, J., Shaw, J.M., and Drews, G.N. (2002). Mitochondrial GFA2 is required for synergid cell death in Arabidopsis. Plant Cell **14,** 2215–2232.

Drews, G.N., Lee, D., and Christensen, C.A. (1998). Genetic analysis of female gametophyte development and function. Plant Cell **10,** 5–17.

Eggermont, K., Goderis, I.J., and Broekaert, W.F. (1996). High-throughput RNA extraction from plant samples based on homogenisation by reciprocal shaking in the presence of a mixture of sand and glass beads. Plant Mol. Biol. Rep. **14,** 273–279.

Eicks, M., Maurino, V., Knappe, S., Flügge, U.I., and Fischer, K. (2002). The plastidic pentose phosphate translocator represents a link between the cytosolic and the plastidic pentose phosphate pathways in plants. Plant Physiol. **128,** 512–522.

Entwistle, G., and ap Rees, T.A. (1988). Enzymic capacities of amyloplasts from wheat (*Triticum aestivum*) endosperm. Biochem. J. **255,** 391–396.

Fischer, K., Kammerer, B., Gutensohn, M., Arbinger, B., Weber, A., Häusler, R.E., and Flügge, U.I. (1997). A new class of plastidic phosphate translocators: A putative link between primary and secondary metabolism by the phosphoenolpyruvate/phosphate antiporter. Plant Cell **9,** 453–462.

Fischer, K., and Weber, A. (2002). Transport of carbon in non-green plastids. Trends Plant Sci. **7,** 345–351.

Flügge, U.I. (1999). Phosphate translocators in plastids. Annu. Rev. Plant Physiol. Plant Mol. Biol. **50,** 27–45.

Forsthoefel, N.R., Wu, Y., Schulz, B., Bennett, M.J., and Feldmann, K.A. (1992). T-DNA insertion mutagenesis in *Arabidopsis*: Prospects and perspectives. Aust. J. Plant Physiol. **19,** 353–366.

Hedrich, R., Raschke, K., and Stitt, M. (1985). A role for fructose-2,6-bisphosphate in regulating carbohydrate metabolism in guard cells. Plant Physiol. **79,** 977–982.

Hellens, R.P., Edwards, E.A., Leyland, N.R., Bean, S., and Mullineaux, P.M. (2000). pGreen: A versatile and flexible binary Ti vector for *Agrobacterium*-mediated plant transformation. Plant Mol. Biol. **42,** 819–832.

Hicks, G.R., Rojo, E., Hong, S., Carter, D.G., and Raikhel, N.V. (2004). Geminating pollen has tubular vacuoles, displays highly dynamic vacuole biogenesis, and requires *VACUOLESS1* for proper function. Plant Physiol. **134,** 1227–1239.

Höfgen, R., and Willmitzer, L. (1990). Biochemical and genetic analysis of different patatin isoforms expressed in various organs of potato (*Solanum tuberosum*). Plant Sci. **66,** 221–230.

Howden, R., Park, S.K., Moore, J.M., Orme, J., Grossniklaus, U., and Twell, D. (1998). Selection of T-DNA-tagged male and female gametophytic mutants by segregation distortion in *Arabidopsis*. Genetics **149,** 621–631.

Ivashikina, N., Deeken, R., Ache, P., Kranz, E., Pommerrenig, B., Sauer, N., and Hedrich, R. (2003). Isolation of *AtSUC2* promoter-GFP-marked companion cells for patch-clamp studies and expression profiling. Plant J. **36,** 931–945.

Kammerer, B., Fischer, K., Hilpert, B., Schubert, S., Gutensohn, M., Weber, A., and Flügge, U.I. (1998). Molecular characterization of a carbon transporter in plastids from heterotrophic tissues: The glucose 6-phosphate/phosphate antiporter. Plant Cell **10,** 105–117.

Knappe, S., Flügge, U.I., and Fischer, K. (2003a). Analysis of the plastidic phosphate translocator gene family in Arabidopsis and identification of new phosphate translocator-homologous transporters, classified by their putative substrate-binding site. Plant Physiol. **131,** 1178–1190.

Knappe, S., Löttgert, T., Schneider, A., Voll, L., Flügge, U.I., and Fischer, K. (2003b). Characterization of two functional *phosphoenolpyruvate/phosphate translocator* (*PPT*) genes in Arabidopsis: *AtPPT1* may be involved in the provision of signals for correct mesophyll development. Plant J. **36,** 411–420.

Kofler, H., Häusler, R.E., Schulz, B., Gröner, F., Flügge, U.I., and Weber, A. (2000). Molecular characterisation of a new mutant allele of the plastid *phosphoglucomutase* in *Arabidopsis*, and complementation of the mutant with the wild-type cDNA. Mol. Gen. Genet. **263,** 978–986.

Konieczny, A., and Ausubel, F.M. (1993). A procedure for mapping *Arabidopsis* mutations using co-dominant ecotype-specific PCR-based markers. Plant J. **4,** 403–410.

Kruger, N.J., and von Schaewen, A. (2003). The oxidative pentose phosphate pathway: Structure and organisation. Curr. Opin. Plant Biol. **6,** 236–246.

Li, Y., Rosso, M.G., Strizhov, N., Viehoever, P., and Weisshaar, B. (2003). GABI-Kat SimpleSearch: A flanking sequence tag (FST)

database for the identification of T-DNA insertion mutants in *Arabidopsis thaliana*. Bioinformatics **19,** 1441–1442.

Lin, T.-P., Caspar, T., Somerville, C., and Preiss, J. (1988). Isolation and characterization of a starchless mutant of *Arabidopsis thaliana* (L.) lacking ADPglucose pyrophosphorylase activity. Plant Physiol. **86,** 1131–1135.

Liu, Y.G., Mitsukawa, N., Oosumi, T., and Whittier, R.F. (1995). Efficient isolation and mapping of *Arabidopsis thaliana* T-DNA insert junctions by thermal asymmetric interlaced PCR. Plant J. **8,** 457–463.

Loddenkötter, B., Kammerer, B., Fischer, K., and Flügge, U.I. (1993). Expression of the functional mature chloroplast triose phosphate translocator in yeast internal membranes and purification of the histidine-tagged protein by a single metal-affinity chromatography step. Proc. Natl. Acad. Sci. USA **90,** 2155–2159.

Mansfield, S.G., and Briarty, L.G. (1992). Cotyledon cell-development in *Arabidopsis thaliana* during reserve deposition. Can. J. Bot. **70,** 151–164.

Martinez, P., Lopez, C., Roldan, M., Sabater, B., and Martin, M. (1997). Plastid DNA of five ecotypes of *Arabidopsis thaliana*: Sequence of *ndhG* gene and maternal inheritance. Plant Sci. **123,** 113–122.

Martinez-Zapater, J.M., Gil, P., Capel, J., and Somerville, C.R. (1992). Mutations at the Arabidopsis *CHM* locus promote rearrangements of the mitochondrial genome. Plant Cell **4,** 889–899.

Mascarenhas, J.P. (1989). The male gametophyte of flowering plants. Plant Cell **1,** 657–664.

McCormick, S. (2004). Control of male gametophyte development. Plant Cell **16** (suppl.), S142–S153.

Mou, Z., He, Y., Dai, Y., Liu, X., and Li, J. (2000). Deficiency in fatty acid synthase leads to premature cell death and dramatic alterations in plant morphology. Plant Cell **12,** 405–418.

Nagata, N., Saito, C., Sakai, A., Kuroiwa, H., and Kuroiwa, T. (1999). The selective increase or decrease of organellar DNA in generative cells just after pollen mitosis one controls cytoplasmic inheritance. Planta **209,** 53–65.

Ohlrogge, J., and Browse, J. (1995). Lipid biosynthesis. Plant Cell **7,** 957–970.

Overlach, S., Diekmann, W., and Raschke, K. (1993). Phosphate translocator of isolated guard-cell chloroplasts from *Pisum sativum* L. transports glucose-6-phosphate. Plant Physiol. **101,** 1201–1207.

Park, S.K., Howden, R., and Twell, D. (1998). The *Arabidopsis thaliana* gametophytic mutation *gemini pollen1* disrupts microspore polarity, division asymmetry and pollen cell fate. Development **125,** 3789–3799.

Piffanelli, P., Ross, J.H., and Murphy, D.J. (1997). Intra- and extracellular lipid composition and associated gene expression patterns during pollen development in *Brassica napus*. Plant J. **11,** 549–562.

Piffanelli, P., Ross, J.H., and Murphy, D.J. (1998). Biogenesis and function of the lipidic structures of pollen grains. Sex. Plant Reprod. **11,** 65–80.

Quick, W.P., Scheibe, R., and Neuhaus, H.E. (1995). Induction of hexose-phosphate translocator activity in spinach chloroplasts. Plant Physiol. **109,** 113–121.

Reiser, L., and Fischer, R.L. (1993). The ovule and the embryo sac. Plant Cell **5,** 1291–1301.

Reynolds, E.S. (1963). The use of lead citrate at high pH as an electron-opaque stain in electron microscopy. J. Cell Biol. **17,** 208–212.

Röbbelen, G. (1966). Chloroplast differentiation following gene induced plastom mutation in *Arabidopsis thaliana* (L.). Heynh. Z. Pflanzenphysiol. **55,** 387–403.

Ruuska, S.A., Girke, T., Benning, C., and Ohlrogge, J.B. (2002). Contrapuntal networks of gene expression during Arabidopsis seed filling. Plant Cell **14,** 1191–1206.

Sambrook, J., Fritsch, E.F., and Maniatis, T. (1989). Molecular Cloning: A Laboratory Manual, 2nd ed. (Cold Spring Harbor, NY: Cold Spring Harbor Laboratory Press).

Sanders, P.M., Bui, A.Q., Weterings, K., McIntire, K.N., Hsu, Y., Lee, P.Y., Truong, M.T., Beals, T.B., and Goldberg, R.B. (1999). Anther developmental defects in *Arabidopsis thaliana* male-sterile mutants. Sex. Plant Reprod. **11,** 297–322.

Schneider, A., Häusler, R.E., Kolukisaoglu, U., Kunze, R., van der Graaff, E., Schwacke, R., Catoni, E., Desimone, M., and Flügge, U.I. (2002). An *Arabidopsis thaliana* knock-out mutant of the chloroplast triose phosphate/phosphate translocator is severely compromised only when starch synthesis, but not starch mobilisation is abolished. Plant J. **32,** 685–699.

Sussman, M.R., Amasino, R.M., Young, J.C., Krysan, P.J., and Austin-Phillips, S. (2000). The Arabidopsis knockout facility at the University of Wisconsin-Madison. Plant Physiol. **124,** 1465–1467.

Twell, D., Park, S.K., and LaLanne, E. (1998). Asymmetric division and cell-fate determination in developing pollen. Trends Plant Sci. **3,** 305–310.

Vaux, D.L., and Korsmeyer, S.J. (1999). Cell death in development. Cell **96,** 245–254.

Yadegari, R., and Drews, G.N. (2004). Female gametophyte development. Plant Cell **16** (suppl.), S133–S141.

Yamamoto, Y., Nishimura, M., Hara-Nishimura, I., and Noguchi, T. (2003). Behavior of vacuoles during microspore and pollen development in *Arabidopsis thaliana*. Plant Cell Physiol. **44,** 1192–1201.

Yu, T.S., Lue, W.L., Wang, S.M., and Chen, J. (2000). Mutation of Arabidopsis plastid phosphoglucose isomerase affects leaf starch synthesis and floral initiation. Plant Physiol. **123,** 319–326.

Zheng, Z., Xia, Q., Dauk, M., Shen, W., Selvaraj, G., and Zou, J. (2003). Arabidopsis AtGPAT1, a member of the membrane-bound glycerol-3-phosphate acyltransferase gene family, is essential for tapetum differentiation and male fertility. Plant Cell **15,** 1872–1887.

Zimmermann, P., Hirsch-Hoffmann, M., Hennig, L., and Gruissem, W. (2004). GENEVESTIGATOR. Arabidopsis microarray database and analysis toolbox. Plant Physiol. **136,** 2621–2632.